INVESTIGATING INCREASED INSULIN SECRETION UPON CASP1/RIPK3 INHIBITION/DELETION

MADISON GIROUARD

Thesis submitted to the University of Ottawa
in partial Fulfillment of the requirements for the
Master of Science in Biochemistry

Department of Biochemistry, Microbiology, and Immunology
Faculty of Medicine
University of Ottawa

Abstract

Inflammation and intrinsic cell death pathways contribute to the pathology of type 2 diabetes (T2D) by promoting β-cell dysfunction and impairing insulin secretion. In its canonical form, Caspase-1 (Casp1) and other inflammasome components work together to activate proinflammatory cytokine release, while receptor-interacting protein kinase 3 (Ripk3) participates in the programmed cell death pathway, necroptosis. Our previous work demonstrated that male and female whole-body Casp1/11 and Ripk3 double knockout (DKO) mice fed a low-fat diet (LFD) exhibited improved glucose tolerance and enhanced glucose-stimulated insulin secretion (GSIS). Here, we investigated mechanisms underlying this phenotype using genetic and pharmacological approaches. Firstly, despite minimal differences in transcriptomic changes in key β-cell target genes between genotypes, immunofluorescence staining of DKO pancreatic sections revealed a reduction in urocortin-3 (UCN3) area. This suggests a potential disruption of the UCN3-somatostatin negative feedback loop, which normally inhibits insulin secretion. We then determined that the non-canonical pyroptosis mediator Casp11 does not contribute to the observed glucose phenotype in DKO mice. Next, using selective Casp1 and Ripk3 inhibitors in mice and isolated islets, we observed increased glucose tolerance and GSIS, similar to those observed in the genetic model. Finally, we found that administration of exogenous UCN3 produced a blunted response in DKO mice, an effect not observed with the addition of the somatostatin analogue octreotide, suggesting that deletion of Casp1 and Ripk3 alters δ-cell function. Understanding how Casp1 and Ripk3 together contribute to glucose metabolism and islet function under LFD conditions can help define their non-canonical roles in the absence of chronic inflammation.

Acknowledgements

I want to take the opportunity to first thank my supervisor, Dr. Morgan Fullerton, for his support and guidance throughout my time in the lab. The positive lab environment that he has fostered is what initially sparked my interest in pursuing graduate studies. I'm especially grateful for his continuous trust in me throughout this project. His leadership and mentoring style are something I truly admire. This project wouldn't have been possible without the collaboration between the labs of Dr. Jenny Bruin and Dr. Erin Mulvihill. I'm especially grateful to Myriam, Cassie, and Lili for welcoming me into the islet community. Your willingness to share your time and expertise made even the most challenging moments feel much more manageable. I also want to thank my thesis advisory committee (TAC) members, Dr. Erin Mulvihill and Dr. Jenny Bruin, for their continuous support and feedback on this project. Your knowledge and feedback truly helped push this project forward. Finally, I would like to acknowledge the incredible members of the Immunometabolab who have been an important part of my journey as a researcher. Thank you, Victoria, Conor, Tyler, Peyman, Julia, Sarah, Ivy, and Mariam for making the lab a place filled with learning, collaboration, and so much laughter.

Table of Contents

List of Tables

List of Figures

Abbreviations

AUC	Area under the curve
BSA	Bovine serum albumin
CANTOS	Canakinumab anti-inflammatory thrombosis outcome study
CASP1	Caspase-1
CKO	Casp1/11 knockout
CLAMS	Comprehensive laboratory animal monitoring system
CRHR2	Corticotropin-releasing hormone receptor 2
DAPI	4′,6-diamidino-2-phenylindole
DKO	Double-knockout
DM	Diabetes mellitus
DMSO	Dimethyl sulfoxide
EDTA	Ethylenediaminetetraacetic acid
EIA	Enzyme immunoassay
ELISA	Enzyme-linked immunosorbent assay
FBS	Fetal Bovine Serum
GABA	Gamma-aminobutyric acid
GCG	Glucagon
GCK	Glucokinase
GD	Gestational diabetes
GLP-1R	Glucagon-like peptide-1 receptor
GLUT1	Glucose transporter type 1
GSIS	Glucose-stimulated insulin secretion
GTT	Glucose tolerance test
HBSS	Hank's balanced salt solution
HFD	High-fat diet
HG	High glucose
IAPP	Islet amyloid polypeptide
IF	Immunofluorescence
IGF	Insulin-like growth factor
IgG	Immunoglobulin G
IL	Interleukin
INS	Insulin
INS1	Rat insulinoma β-cell line
IP	Intraperitoneal
IRS	Insulin receptor substrate
ITT	insulin tolerance test
KO	Knockout
KRBH	Krebs-Ringer bicarbonate
LFD	Low-fat diet
LG	Low glucose
LPS	Lipopolysaccharide
MafA	Musculoaponeurotic fibrosarcoma oncogene family A
NASH	Non-alcoholic steatohepatitis
NLRP3	NOD-like receptor family pyrin domain-containing 3

NOD	Nucleotide-binding and oligomerization domain
oGTT	Oral glucose tolerance test
PBS	Phosphate-Buffered Saline
PI3K	Phosphatidylinositol 3-kinases
PP	Pancreatic polypeptide
RIPK3	Receptor-interacting serine/threonine-protein kinase 3
RKO	Ripk3 knockout
ROS	Reactive oxygen species
RPMI	Roswell Park Memorial Institute
SST	Somatostatin
SSTR2	Somatostatin receptor type 2
T1D	Type 1 diabetes
T2D	Type 2 diabetes
TCRs	T cell receptors
TLRs	Toll-like receptors
TNFs	Tumour necrosis factors
UCN3	Urocortin 3
VEGF	Vascular endothelial growth factor A
WAT	White adipose tissue
WT	Wild-type

Chapter 1: Introduction

1.1 Diabetes and glucose homeostasis

1.1.1 Diabetes mellitus in Canada

Diabetes mellitus (DM) is a chronic metabolic disorder that gradually impairs the body's ability to maintain glucose homeostasis (1). Although there are many classifications of DM, the main forms that affect Canadians are type 1 diabetes (T1D), type 2 diabetes (T2D), and gestational diabetes (GD) (2). GD occurs during pregnancy, usually stemming from insulin resistance with an insufficient compensatory insulin response to hormonal changes and the metabolic requirements of a growing fetus (3). In comparison, T1D is an autoimmune condition in which the body's immune system destroys the insulin-producing β-cells of the pancreas, leaving individuals dependent on lifelong insulin therapy (4).

Among the various forms, T2D is by far the most common, making up roughly 90-95% of all diabetes cases in Canada (2). It develops gradually, often over many years, as the body becomes less able to produce enough insulin or use the insulin it produces as effectively (5). As of 2024, around 10% of Canadians were living with either T1D or T2D (6). For those with T2D, the long-term health risks can be significant, including cardiovascular disease, nephropathy, neuropathy, retinopathy and increased risk of infections (7). A key challenge for researchers is that T2D does not stem from a single cause but is generally believed to result from a combination of genetic predisposition, physical inactivity, dietary patterns, and broader socio-economic factors (8). Compounding this issue, the prevalence of T2D in Canada has been increasing at an average rate of 3.3% annually (9), placing growing pressure on healthcare systems through increased costs and overburdened care services. Altogether, it has become clear that T2D is a growing public health challenge that requires ongoing research and the development of novel therapies.

1.2 Pancreatic islets

1.2.1 Endocrine cell types

The pancreas consists of exocrine and endocrine regions. While the exocrine region primarily supports digestive functions, emerging evidence suggests signalling and crosstalk between exocrine and endocrine compartments contribute to the regulation of glucose homeostasis (10). The endocrine pancreas contains islets of Langerhans, which secrete hormones to maintain blood glucose levels (11). There are five different endocrine cell types, including α-cells that secrete glucagon, β-cells that secrete insulin, δ-cells that secrete somatostatin, ε-cells that secrete ghrelin, and finally PP-cells (sometimes known as F cells) that secrete pancreatic polypeptides (12). Importantly, human and rodent islets differ in their organization and cell-type composition (13). While keeping inter-islet variability in mind, humans generally have a lower proportion of β-cells (50-60%) and a higher proportion of α-cells (30-50%) compared with rodent islets (65-80% and 10-20%, respectively) (14). Both human and rodent δ-cells typically account for around 5%, and ε-cells/pancreatic polypeptide (PP) cells account for less than 1% of the total (14).

1.2.2 Intra-islet paracrine communication

The close arrangement of cells within islets allows for essential paracrine signalling by releasing hormones and neurotransmitters into the interstitial space (15). In response to glucose, mature rodent β-cells co-release insulin and the hormone peptide urocortin 3 (UCN3). While in humans, both mature β- and α-cells release UCN3 (16). Once released, UCN3 binds to the corticotropin-releasing hormone receptor 2 (Crhr2) found on the δ-cell (17). In response, activated δ-cells secrete somatostatin, a potent hormone that provides negative feedback inhibition on both insulin (β-cells) and glucagon (α-cells) (Figure 1) (16). In addition to insulin and UCN3, β-cells

co-secrete a variety of factors that shape intra-islet signalling. For example, islet amyloid polypeptide (IAPP, or amylin) inhibits glucagon secretion and slows gastric emptying (18–20). However, in T2D, IAPP misfolding leads to islet amyloid deposits that contribute to β-cell loss and islet dysfunction (21,22). Fast neurotransmitters and neuromodulators such as gamma-aminobutyric acid (GABA) (23), glutamate (24), and serotonin (25) help regulate β- and α-cell activity and β-cell mass. β-cells produce growth and vascular factors, such as vascular endothelial growth factor A (VEGF-A) and members of the insulin-like growth factor (IGF) family, to support islet structure and survival (26,27). Under stress, β-cells can release proinflammatory cytokines such as Interleukin-1β (IL-1β), IL-6 and other signals that activate local immune responses (28,29). Overall, the coordination of hormone outputs functions as an integrated signalling network to ensure glucose homeostasis.

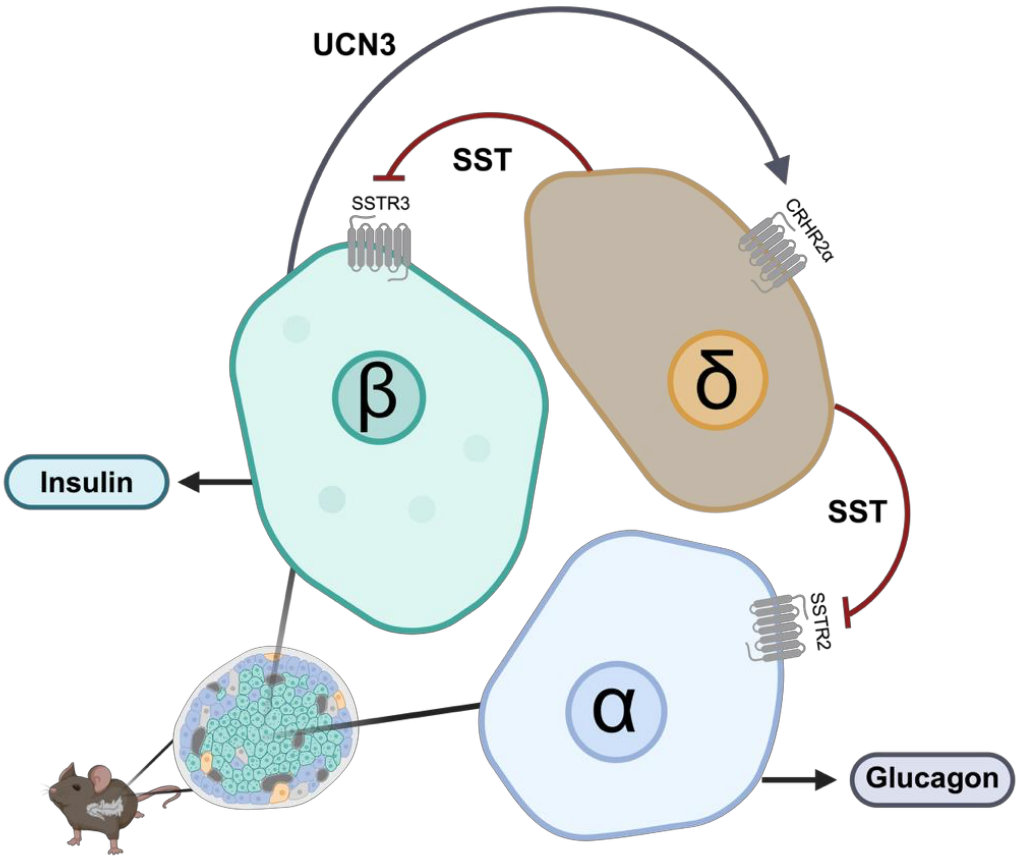

Figure 1. Paracrine islet hormone signalling network in rodents.
Schematic of interactions among glucagon-secreting α-cells, insulin-secreting β-cells, and somatostatin-secreting δ-cells. In response to elevated glucose, β-cells release insulin and UCN3. UCN3 acts on CRHR2α on δ-cells to stimulate somatostatin (SST) release, which provides a local inhibitory signal to both α- and β-cell secretion on the somatostatin receptor type 2 (SSTR2) and SSTR3, respectively. Adapted from Flisher et al., Peptides (2022) (30).

1.2.3 Glucose sensing and β-cell insulin secretion

Pancreatic β-cells play an important role in regulating glucose homeostasis by secreting insulin. More specifically, they are responsible for the synthesis, storage and release of insulin while also acting as glucose sensors (31). In brief, circulating glucose enters β-cells via glucose transporters (primarily glucose transporter type 1 (GLUT1) in humans and GLUT2 in rodents) (32). Next, the glucose is phosphorylated by the glucose-sensing enzyme, glucokinase (GCK) and metabolized through glycolysis and oxidative phosphorylation to produce ATP (33). An increase in ATP leads to a higher ATP/ADP ratio, which closes ATP-sensitive potassium channels (34). This induces membrane depolarization and subsequent calcium (Ca^{2+}) influx, which allows insulin-containing secretory granules to be released by exocytosis into the bloodstream (14,33). Alternatively, insulin can be stored within the secretory vesicles in crystalline form (34).

1.2.4 Dysregulation of insulin secretion in metabolic syndrome

T2D is often accompanied by metabolic syndrome, an umbrella term for a cluster of conditions including hypertension, elevated fasting glucose, dyslipidemia, and central adiposity (35). Chronic stressors such as overnutrition and physical inactivity promote insulin resistance and compensatory hyperinsulinemia, ultimately placing increased demand on β-cells and leading to their dysfunction (36,37). Excess nutrient supply is known to promote ectopic lipid accumulation and the accumulation of lipotoxic mediators (e.g. diacylglycerols and ceramides) in insulin-sensitive tissues, leading to defects in insulin receptor/insulin receptor substrate (IRS)-phosphoinositide 3-kinase (PI3K)-protein kinase B (Akt) signalling and hindering glucose uptake (38–41). In parallel, chronic hyperglycemia activates glucotoxic pathways, including advanced glycation end-product formation and increased oxidative metabolism, worsening insulin resistance

and β-cell stress (42–45). Prolonged β-cell stress drives multiple cellular dysfunctions, including oxidative stress/reactive oxygen species (ROS) accumulation, mitochondrial dysfunction, inflammation, and cell death (46–48). Functionally, these stress pathways lead to impaired insulin secretion and loss of functional β-cell mass (49,50). Overall, these findings underscore the central importance of β-cell function in preserving glucose homeostasis.

1.3 Inflammasome signalling

1.3.1 Inflammasome activation pathways

During chronic nutrient excess, an expansion of adipose tissue occurs through the increase of adipocytes (hypertrophy) as well as the proliferation and differentiation of adipose precursor cells (hyperplasia) (51). Adipose tissue eventually becomes stressed due to increased oxygen and nutrient demands (52). This leads to the release of proinflammatory cytokines, including IL-1β and IL-18, causing inflammation and insulin resistance (53,54). However, before they can be released, IL-1β and IL-18 must first be activated from their inactive precursors by the intracellular cysteine protease Caspase-1 (Casp1) (55,56). Casp1 functions within a large multiprotein complex called the inflammasome, which consists of a sensor protein and an adapter protein, apoptosis-associated speck-like protein with caspase recruitment domain (57). A range of exogenous and endogenous stressors activate different sensor proteins (58). While there are many different types of inflammasome complexes, the nucleotide-binding and oligomerization domain (NOD)-like receptor family pyrin domain-containing 3 (NLRP3) inflammasome is the most well-studied inflammasome (59) and is known to become activated during high glucose conditions (60). Specifically, a study by Wen et al. demonstrated that high-fat diet-fed NLRP3-deficient mice were more glucose tolerant, insulin sensitive, and showed increased insulin signalling in key tissues,

including the liver, muscle, and white adipose tissue (WAT) (61). Overall, this suggests that NLRP3 inflammasome activation promotes insulin resistance. In addition to canonical inflammasome activation mediated by Casp1, a non-canonical pathway exists in which Casp11 (Casp4 and Casp5 in humans) directly binds to lipopolysaccharide (LPS) from gram-negative bacteria, causing a form of inflammatory cell death (pyroptosis) and inflammatory signalling (62). While Casp1 acts within inflammasome complexes such as NLRP3, Casp11 functions independently of these sensors, suggesting that they have different roles in innate immune signalling (63,64).

1.3.2 Casp1 in inflammation and metabolic disease

Beyond its canonical inflammatory role, Casp1 exhibits broad substrate specificity spanning metabolism, cell death, and cytoskeletal function (65). Currently, research on the role of Casp1 and its implications in obesity and metabolism in mice is conflicting. Researchers have demonstrated that Casp1-deficient mice are more sensitive to insulin (53) and that mice fed a HFD treated with a pharmacological Casp1 inhibitor (Ac-YVAD-cmk) prevented the progression of insulin resistance, liver fibrosis, and non-alcoholic steatohepatitis (NASH) (66). In comparison, other studies have suggested that a Casp1 deletion/inhibition has the opposite effect (67–69). For example, a study by Wang et al. found that reduced circulating IL-18 levels in Casp1-deficient mice led to greater obesity and insulin resistance on a HFD than in wild-type (WT) mice (67).

In humans, Dominy et al. found that individuals with a complete loss of Casp1 had dramatically reduced levels of proinflammatory cytokines IL-1β and IL-18, along with lower neutrophil counts. However, these individuals showed no obvious clinical abnormalities and were not more susceptible to recurrent infections (70). In a different study, Palomäki et al. reported that

in humans with obesity and insulin resistance, Casp1 is highly expressed in adipose-tissue macrophages within crown-like structures. Following bariatric surgery, Casp1 expression and activity in these cells declined concomitantly with improvements in metabolic health, highlighting the contributions of the NLRP3-Casp1 axis to obesity-related metabolic dysfunction (71). Finally, in a large clinical trial called the Canakinumab Anti-inflammatory Thrombosis Outcome Study (CANTOS) (2011-2017), researchers investigated the use of canakinumab, an antibody targeting IL-1β. While the trial demonstrated dose-dependent improvements in cardiovascular outcomes following canakinumab treatment, blocking inflammation alone was not enough to prevent the progression of T2D (72).

1.4 Cell death signalling

1.4.1 Necroptosis and other cell death pathways

T2D is characterized not only by chronic inflammation but also by the activation of multiple cell death pathways. Cells can either die in a programmed or unprogrammed manner, with or without the release of additional inflammatory responses. Apoptosis is an extensively studied and well-understood form of non-inflammatory regulated cell death, involving stimulated initiator caspases (e.g. Casp8 and -9) that trigger proteolytic stimulation of effector caspases (e.g. Casp3 and -7) in a cascade-like manner (73–75). Apoptosis is activated automatically when cells do not receive pro-survival factors or when extracellular signals indicate a potential threat to the host organism (74). In contrast, necrosis is a well-known rapid, non-programmed form of cell death that occurs in response to internal or external stresses, such as mechanical injury, chemical agents, or pathogens (76). Cell lysis occurs due to plasma membrane swelling and loss of integrity during necrosis (77,78). Inevitably, some harmful intracellular contents can damage nearby cells,

triggering an inflammatory response (74). Later, researchers defined a cell death pathway that occurs in a more regulated manner than necrosis and exhibits highly immunogenic characteristics. Necroptosis is a programmed form of cell death that triggers inflammation and has various roles in both physiological and pathological conditions (79). Receptor-interacting protein kinase 1 (Ripk1), Ripk3, and mixed lineage kinase domain-like protein (Mlkl) make up the necrosome, which is responsible for rupturing the cell membrane from within (79). Necroptosis is activated upon signals from tumour necrosis factors (TNFs), Toll-like receptors (TLRs), or T cell receptors (TCRs) when apoptotic Casp8 is inhibited (80). Another inflammatory form of cell death, called pyroptosis, which is often triggered by pathogens, stroke, heart attack, or cancer, is activated by Casp1/11 in mice (Casp1, 4, 5 in humans) to cause osmotic lysis (81).

1.4.2 Ripk3 and links to metabolic disease

Although Ripk1-deficient mice are not viable, Ripk3-deficient mice are viable, and numerous studies have investigated Ripk3's role in metabolic disease (80). Currently, researchers are aware that necroptosis is recognized as a contributor to various pathological conditions such as acute kidney injury (82), atherosclerosis (83), neurodegenerative disease (84), and diabetes (85). Moreover, a study by Yang et al. demonstrated that a Ripk3 inhibitor (GSK'872) prevented β-cell loss in muscle insulin-resistant zebrafish, suggesting a role for Ripk3 in overnutrition-induced β-cell loss and dysfunction (86). The authors proposed that ER stress in β-cells induced by HFD activates Ripk3 and promotes IL-1β release, which then recruits macrophages to the islet, contributing to islet inflammation and β-cell dysfunction (86). While Ripk3 represents a compelling therapeutic target, human studies within metabolic disease remain limited.

1.5 Metabolic phenotype of Casp1/11/Ripk3 DKO mice

1.5.1 Body weight

Previous work by our collaborator, Dr. Subash Sad, generated a mouse model deficient in Casp1/Casp11/Ripk3 to investigate host defence mechanisms against *Salmonella enterica* serovar Typhimurium infection. While his group demonstrated that Ripk3 plays a protective role in host defence, particularly when Casp1/11 signalling is absent, this study raised questions about whether Ripk3 might have broader physiological functions beyond its role in inflammatory cell death (87).

In previous studies conducted in our lab, the Casp1/11/Ripk3 double-knockout (DKO) mice were fed either a standardized low-fat diet (LFD; 10% kcal from fat) or a high-fat diet (HFD; 60% kcal from fat) for 14 weeks. No differences in body weight were observed between genotypes in either sex for LFD mice (Figure 2B, C). In male and female HFD mice, baseline weights were not different at the start, but over several weeks on the diet, DKO mice showed greater weight gain (Figure 3BC).

1.5.2 Glucose tolerance and insulin sensitivity

During the 14-week dietary interventions, glucose tolerance was assessed using a glucose tolerance test (GTT), which measures the body's ability to clear glucose from the bloodstream following a glucose challenge. Insulin sensitivity was determined by the insulin tolerance test (ITT) by monitoring the decline in blood glucose in response to insulin. Under LFD conditions, single Casp1/11 and Ripk3 KO mice showed glucose tolerance comparable to WT controls, but DKO mice displayed improved glucose tolerance in both sexes (Figure 2D, E). Insulin sensitivity was not different between genotypes in either sex, suggesting that the improved glucose tolerance observed in DKO mice occurred independently of changes in insulin sensitivity (Figure 2F, G).

Interestingly, under HFD conditions, a different phenotype emerged. Male DKO and single KO mice had significantly impaired glucose tolerance, and female DKO and KO mice showed no difference in glucose tolerance compared with WT controls (Figure 3D, E). Insulin sensitivity remained unchanged across genotypes in both sexes (Figure 3F, G).

1.5.3 Insulin secretion

Since the improved glucose tolerance observed in LFD mice was not due to changes in insulin sensitivity, insulin secretion was assessed in DKO mice. Serum insulin levels were measured at baseline and 30 minutes after glucose administration, revealing significantly elevated glucose-stimulated insulin secretion (GSIS) in DKO mice compared with WT controls in both sexes (Figure 4A, C). To further investigate the islets themselves, *ex vivo* dynamic insulin secretion assays through perifusion were performed in isolated pancreatic islets from DKO mice at endpoint. In the islets from LFD-fed male DKO mice, both GSIS and depolarization-induced insulin secretion in response to KCl were significantly increased compared with WT controls (Figure 4B, D), indicating an enhanced secretory capacity at the islet level. In islets isolated from LFD-fed female DKO mice, there was a trend toward increased GSIS and a significant increase in KCl-stimulated insulin secretion compared with WT controls. In contrast, under HFD conditions, no differences in GSIS or KCl-stimulated insulin secretion were observed in islets from either sex, suggesting that HFD feeding blunts the enhanced insulin secretory phenotype observed under LFD conditions.

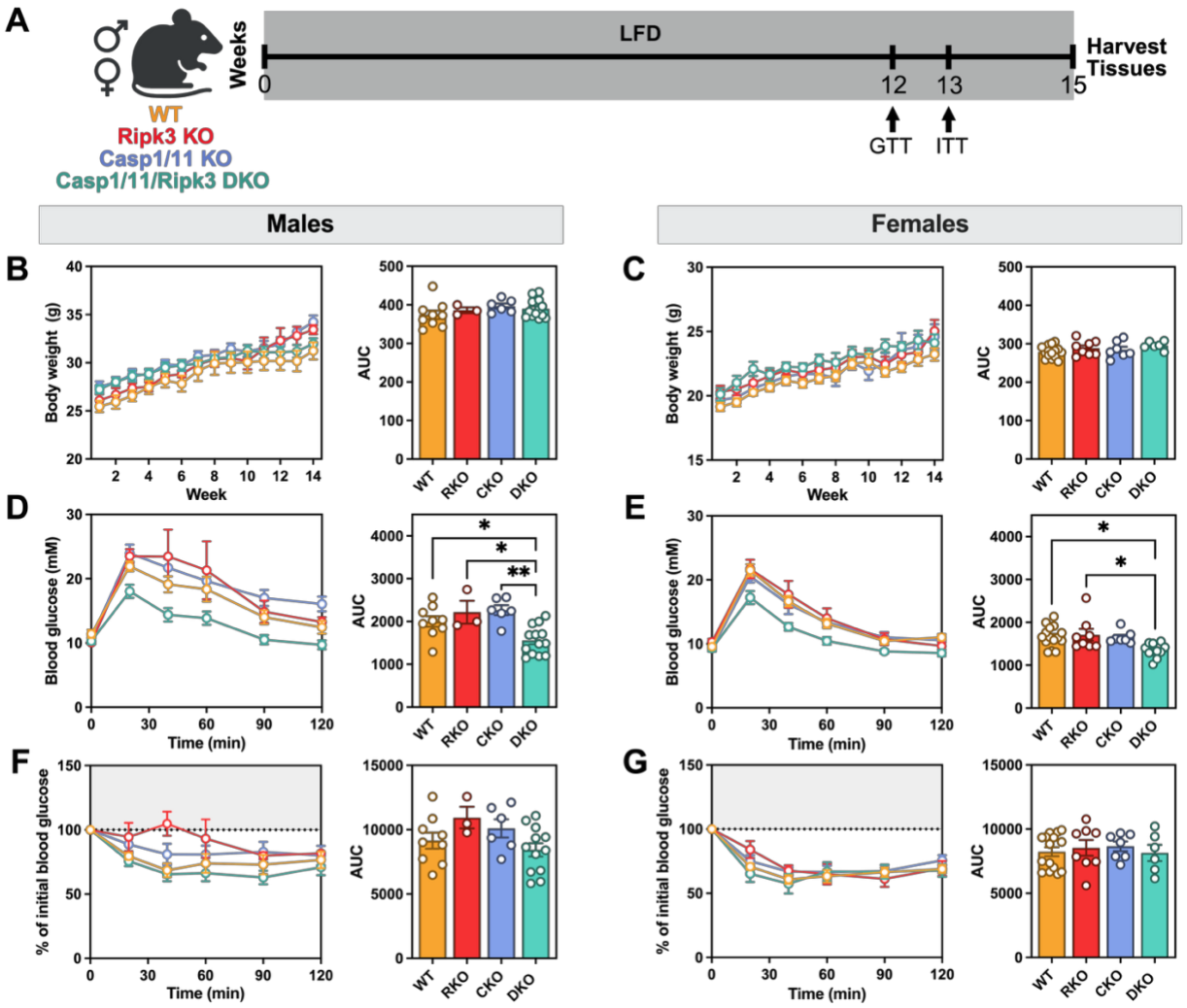

Figure 2. Improved glucose tolerance in LFD-fed Casp1/11/Ripk3 DKO mice.
(A) Experimental timeline for male and female mice fed a LFD (10% kcal from fat). **(B-C)** Body weights of WT, Ripk3 KO (RKO), Casp1/11 KO (CKO), and Casp1/11/Ripk3 (DKO) mice were measured over 14 weeks. **(D-E)** ipGTT (1.5 g/kg glucose in 0.9% saline) was performed on 5-hour fasted mice. Blood glucose levels were measured over 120 minutes. **(F-G)** ipITT (0.5 U/kg insulin) on 4.5-hour fasted mice, with glucose measurements taken over 120 minutes. Data are mean ± SEM (n = 3-15 mice per genotype). Data generated by Conor O'Dwyer. Significance was determined by ordinary one-way ANOVA. *p-value <0.05, **p-value <0.01.

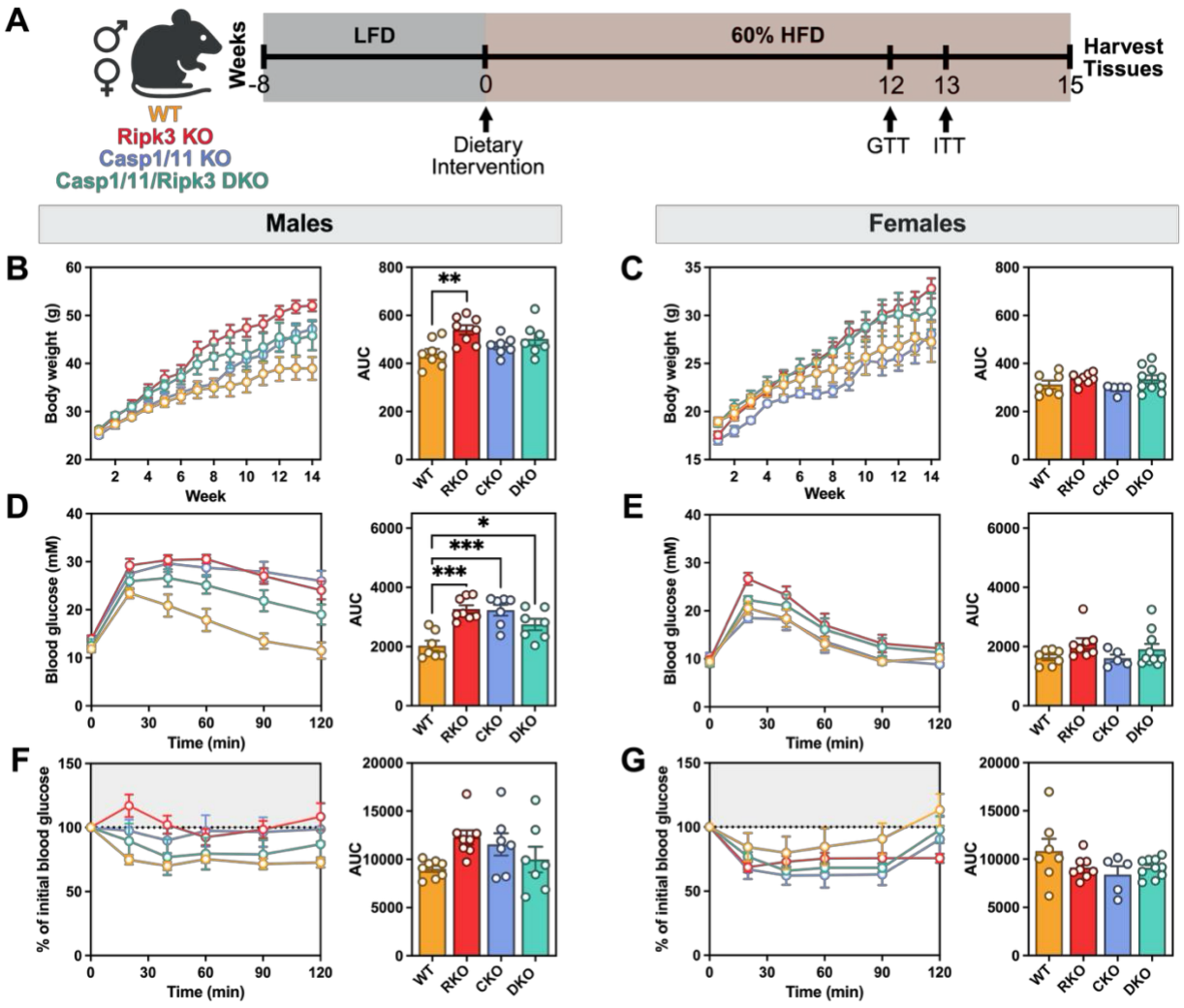

Figure 3. Increased weight gain and glucose intolerance in HFD-fed male Casp1/11/Ripk3 DKO mice.

(A) Experimental timeline for male and female mice fed a HFD (60% kcal from fat). **(B-C)** Body weights of WT, Ripk3 KO (RKO), Casp1/11 KO (CKO), and Casp1/11/Ripk3 (DKO) mice were measured over 14 weeks. **(D-E)** ipGTT (1.5 g/kg glucose in 0.9% saline) was performed on 5-hour fasted mice. Blood glucose levels were measured over 120 minutes. **(F-G)** ipITT (1 U/kg insulin) on 4.5-hour fasted mice, with glucose measurements taken over 120 minutes. Data are mean ± SEM (n = 5-10 mice per genotype). Data generated by Conor O'Dwyer. Significance was determined by ordinary one-way ANOVA. *p-value <0.05, **p-value <0.01, ***p-value <0.001.

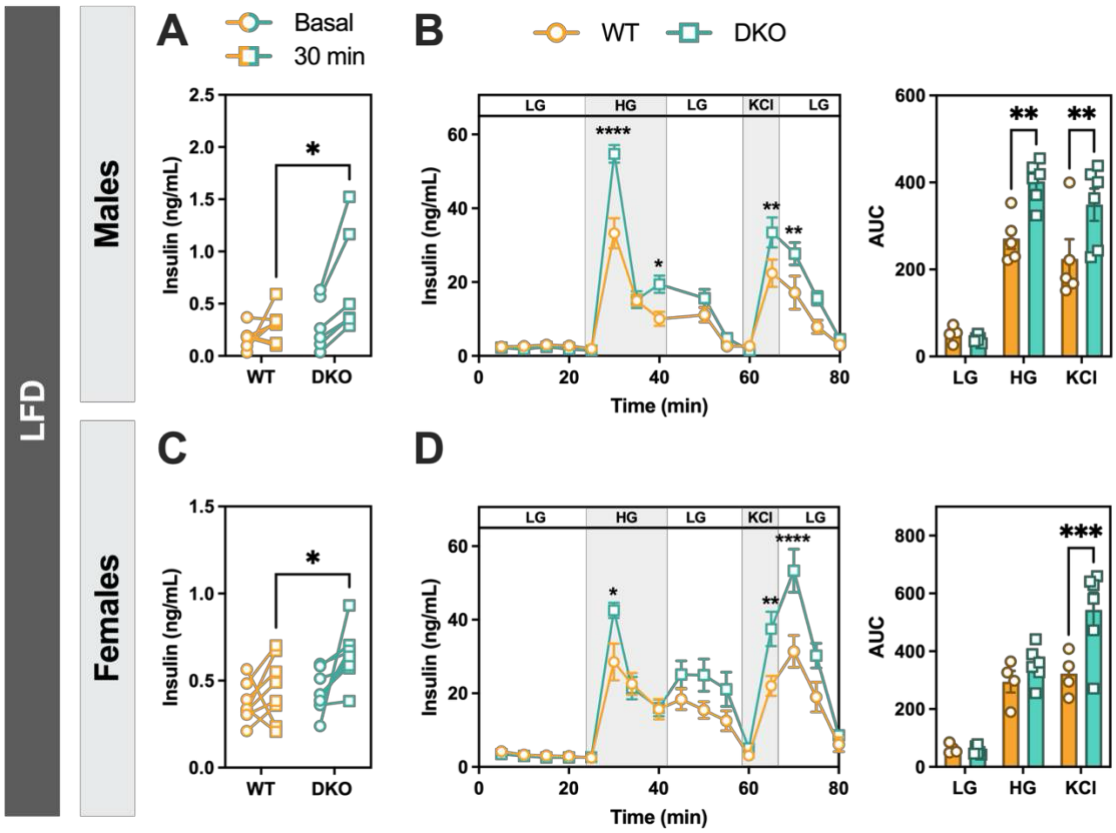

Figure 4. Increased insulin secretion in mice and islets following Casp1/11/Ripk3 deletion. **(A-C)** Serum insulin concentrations were measured before and 30 minutes after ip glucose injection (1.5 g/kg glucose in 0.9% saline) in 5-hour fasted LFD-fed mice. **(B-D)** Dynamic insulin secretion from isolated WT and DKO mouse islets in response to low glucose (LG; 2.8 mM), high glucose (HG; 16.7 mM), and depolarizing potassium (KCl; 30 mM). Insulin release was measured over 80 minutes. Data are mean ± SEM (n = 4-8 mice per genotype). Data generated by Myriam P Hoyeck and Kayleigh R.C. Rick (Carleton University). Significance was determined by two-way ANOVA. *p-value <0.05, **p-value <0.01, ***p-value <0.001, ****p-value <0.0001.

1.6 Hypothesis and objectives

In healthy, non-diabetic mice, immune cells are present at very low levels within islets, typically accounting for only 2.7 ± 1.3% of total islet cells (88). While initially interested in determining the effects of Casp1/11/Ripk3 deletion under metabolic stress and the presence of obesity, the LFD phenotype prompted a different focus. Given that these pathways are typically most active in immune cells and under conditions of metabolic dysfunction or inflammation, it was not expected that their disruption would significantly influence glucose homeostasis in the relatively homeostatic LFD state. These findings suggest that alterations in Casp1/11 and Ripk3 together may regulate β-cell insulin secretory capacity, pointing to a potential non-canonical role for these proteins.

The primary goal of this study was to better understand why/how this phenotype occurs in LFD mice. We hypothesized that paracrine signalling mechanisms within the islets could be influencing glucose homeostasis, though the precise pathways remained to be determined. In addition, we propose that there may be intrinsic alterations within the β-cells themselves that enable a hypersecretion phenotype. To test this, we first characterized markers of islet composition, supporting a UCN3-somatostatin paracrine loop in DKO mice. We next determined the contribution of Casp11 by generating new Casp1/Ripk3 DKO mice to reproduce the phenotype. We examined the effects of pharmacological inhibition of Casp1 and Ripk3, and finally assessed the impact of exogenous UCN3 and somatostatin analog on glucose tolerance and insulin secretion using *ex vivo* and *in vivo* systems.

Chapter 2: Materials and Methods

2.1 Mouse models

To begin, we crossed mice harbouring a whole-body deletion of Casp1 and Casp11, initially generated by Dr. Richard Flavell (89), with mice deficient for Ripk3, initially generated by Dr. Vishwa Dixit (90). Double heterozygous mice were crossed to produce littermate-derived WT, Casp1/11 KO, Ripk3 KO and Casp1/11/Ripk3 DKO mice. To interrogate the relative contributions of the Casp1/11 dual knockout, we also crossed B6.Cg-Casp1^{em1Vnce}/J (91) (JAX#032662) with Ripk3 mice to rederive WT, single and double KO animals. For pharmacological studies, C57BL/6J mice, originally purchased from The Jackson Laboratory (#00664), were bred in-house and backcrossed yearly. All mice were maintained on a C57BL/6J background. Male and female mice were reared on a standard chow diet until 8 weeks of age. At this point, male and female mice were placed on either a standardized LFD (10% kcal from fat, 70% kcal from carbohydrates and 20% kcal from protein; Research Diets Inc, #D12450B) or a HFD (~60% kcal from fat, ~20% kcal from carbohydrates and ~20% kcal from protein; Research Diets Inc, #D12492) for 14 weeks. Mice were group-housed in ventilated cages at ~22°C, maintained on a 12-hour light/dark cycle (lights on at 7 am) with unrestricted access to food and water. Mice were euthanized in the fed state following administration of ketamine (150 mg/kg)-xylazine (10 mg/kg) anesthesia, followed by cervical dislocation. All animal experiments were performed in accordance with the guidelines of the Canadian Council on Animal Care and were approved by the University of Ottawa Animal Care Committee.

2.2 Metabolic assessments

Body weights were recorded weekly throughout the 14-week dietary intervention. Mice were singly housed and acclimated for 24 hours before undergoing indirect calorimetry assessment in a Comprehensive laboratory animal monitoring system (CLAMS; Columbus Instruments) for a further 72 hours. Following data output from the Oxymax software, differences between groups of mice were determined using CalR 2.0 (92).

Blood glucose levels were measured using a handheld glucometer (Accuchek), following introduction of a small cut in the lateral tail vein. Intraperitoneal (ip) glucose tolerance test (ipGTT) or oral GTT was conducted following a 4.5- or 5-hour fast, respectively, beginning at ~9 am. Following basal glucose measurement, mice received 1.5 g/kg (ipGTT) or 2 g/kg (oGTT) D-glucose in saline. Blood glucose concentrations were subsequently measured at 20, 40, 60, 90, and 120 minutes, with blood samples collected in lithium heparin-coated tubes at baseline and 30 minutes for plasma insulin measurements. After blood collection, samples were left to clot at room temperature for approximately 30 minutes and then centrifuged at 10,000 rpm for 5 minutes. The resulting supernatant was collected, and insulin concentrations were measured by enzyme-linked immunosorbent assay (ELISA) (ALPCO, #80-INSMSU-E10). For experiments involving Casp1 and Ripk3 pharmacological inhibition, C57BL/6J mice were administered the Casp1 inhibitor Ac-YVAD-cmk (2.5 mg/kg; Cayman Chemical; #10014) and the Ripk3 inhibitor GSK'872 (2.5 mg/kg; Cayman Chemical; #23300) by ip injection once daily for 2 consecutive days (8 am). Glucose tolerance was assessed by ipGTT on day 2. For Ucn3 experiments, mice received an ip injection of a Ucn3 peptide (10 or 50 nmol/kg; Bachem; #4040194) 5 minutes prior to glucose administration at the indicated concentrations. To mimic somatostatin, Octreotide (25 ug/kg; Cayman Chemical; #23757) was injected (ip) 30 minutes prior to glucose administration.

For insulin tolerance tests (ITT), mice were fasted for 4 hours in the morning (9 am), and basal blood glucose was assessed prior to ip injection of insulin (0.5 U/kg or 1 U/kg) in saline (Novo). Blood glucose concentrations were measured at 20, 40, 60, 90, and 120 minutes following insulin administration.

2.3 Mouse islet isolation

Mouse pancreatic islets were isolated as previously described (93). Briefly, the pancreatic duct was perfused with a collagenase solution (1,000 U/mL; Sigma-Aldrich, #C7657) prepared in Hank's Balanced Salt Solution (HBSS; 137 mM NaCl, 5.4 mM KCl, 4.2 mM NaH_2PO_4, 4.1 mM KH_2PO_4, 10 mM HEPES, 1 mM $MgCl_2$, 5 mM dextrose; pH 7.2) following clamping of the duct at the duodenum. After ductal inflation, the pancreas was excised, cut up, and transferred to conical tubes containing ice-cold HBSS. Samples were digested in a 37°C water bath for 10.5 minutes, after which tubes were vigorously shaken 10-15 times to further dissociate pancreatic tissue. Digestion was immediately quenched by the addition of ice-cold HBSS supplemented with $CaCl_2$ (1 mM). Samples were washed three times in HBSS + $CaCl_2$ with centrifuging in between for 1 minute at 1000 rpm and, after the final wash, tissue was resuspended in Roswell Park Memorial Institute (RPMI) medium (Multicell; #350-000 CL) supplemented with 1% penicillin-streptomycin (Gibco; #15140122) and 10% fetal bovine serum (FBS; Multicell; #090-150). Islets were separated from exocrine tissue using a Histopaque density gradient (Sigma-Aldrich; #10771) and collected using a 70 μm cell strainer. Islets were then hand-picked to ensure purity using a dissecting microscope and cultured overnight at 37°C in supplemented RPMI in a 5% CO_2 incubator to allow recovery.

2.4 RNA isolation, cDNA synthesis and qPCR

Following islet isolation, mouse islets were handpicked and lysed in RLT buffer containing 1% β-mercaptoethanol and stored at -80°C until processing. Total RNA was extracted using TriPure RNA Isolation Reagent (Roche; #11667165001) according to the manufacturer's instructions. RNA concentrations were measured using a Take3 Plate (Agilent; #TAKE3-SN) on a Synergy H1 plate reader (BioTek) and normalized with DNase/RNase-free water prior to transfer into 8-strip PCR tubes. Reverse transcription was performed by adding All-in-One 5× RT Master Mix (Applied Biological Materials; #G592) to each sample, followed by cDNA synthesis according to the manufacturer's protocol. The resulting cDNA was diluted 1:10-1:40, depending on the gene target, in DNase/RNase-free water. qPCR was conducted using QuantiNova Probe PCR Master Mix (Qiagen; #208254) for TaqMan probes, while BlasTaq 2X qPCR Master Mix (Applied Biological Materials; #G891) was used for non-TaqMan probes. Primer sequences are provided in Table 1. Reactions were run on a Rotor-Gene Q system (Qiagen). Relative transcript expression was calculated using the $2^{-\Delta\Delta Ct}$ method (94) with *Ppia* and *Hprt* as housekeeping genes.

Table 1. Primers used in RT-qPCR

Oligos for use with SYBR Green			
Target (mouse)	Forward (5'-3')	Reverse (5'-3')	cDNA dilution for islets
Hprt	GCTGACCTGCTGGATTACAT	TTGGGGCTGTACTGCTTAAC	1:10
Ppia	AGCTCTGAGCACTGGAGAGA	GCCAGGACCTGTATGCTTTA	1:10
Ins1	TCAGAGACCATCAGCAAGCA	CTCCCAGAGGGCAAGCAG	1:100
Ins2	GCTTCTTCTACACACCCATGT	ACGACTGATCTACAATGCCAC	1:100
MafA	AGTCGTGCCGCTTCAAG	CGCCAACTTCTCGTATTTCTCC	1:10
Nkx6.1	CTTCGCCCTGGAGAAGAC	CCGAGTCCTGCTTCTTCTTG	1:10
Ucn3	AAGCCTCTCCCACAAGTTCTA	GAGGTGCGTTTGGTTGTCATC	1:10
Gck	TGGTGGATGAGAGCTCAGTG	TGAGCAGCACAAGTCGTACC	1:10
Slc2a2	GCAACTGGGTCTGCAATTTT	CCAGCGAAGAGGAAGAACAC	1:25
Sst	CTGAGCAGGACGAGATGAGG	TAACAGGATGTGAATGTCTTCCAGAA	1:100
Gcg	ACTCACAGGGCACATTCACC	CCAGTTTATAAAGTCCCTGG	1:100

TaqMan Probes	
Target (mouse)	Assay ID (ThermoFisher Scientific)
Crhr2	Mm00438308_m1

2.5 Immunofluorescence staining and image quantification

Whole pancreata were harvested, fixed in formalin, and processed for paraffin embedding through the Louise Pelletier Histology Core (University of Ottawa). Paraffin-embedded tissue was sectioned at 5 µm thickness using a Leica RM2135 microtome and mounted onto glass slides. Immunofluorescence (IF) staining was conducted as previously described (93). To summarize, tissue sections were first deparaffinized and rehydrated through a series of graded xylene and ethanol washes, followed by a phosphate-buffered saline (PBS) rinse. Heat-induced epitope

retrieval was performed using an EZ Retriever microwave in citrate buffer (10 mM sodium citrate, 0.05% Tween-20; pH 6.0) at 95°C for 10 minutes, while musculoaponeurotic fibrosarcoma oncogene family A (MafA) samples were retrieved in TE buffer (10 mM Tris base, 1 mM EDTA, 0.05% Tween-20; pH 9.0) at 95°C for 15 minutes. A hydrophobic barrier was created around each tissue section using an ImmEdge Pen (Vector Laboratories; #H-4000), and DAKO serum-free protein block (Agilent; #X090930-2) was applied for 30 minutes in a humid chamber. After removing the protein block, primary antibodies were added to the sections and incubated overnight at 4°C. The following day, slides were washed three times with PBS, then incubated with Alexa Fluor-conjugated secondary antibodies for 1 hour at room temperature in a humid chamber. After three additional PBS washes, slides were mounted with Vectashield HardSet mounting medium with DAPI (Vector Laboratories; #H-1500) and left to harden under a coverslip. Primary antibodies were all diluted in Dako Antibody Diluent solution (Agilent; #S202230-2). The following primary antibodies were used: rabbit anti-somatostatin (1:500, Sigma-Aldrich; #HPA019472), mouse anti-insulin (1:250, Cell Signaling; #8138S), mouse anti-glucagon (1:250, Sigma-Aldrich; #G2654-0.2ml), rabbit anti-insulin (1:200, Cell Signaling; #3014), rabbit anti-Ucn3 (1:500, custom antibody generated at the Salk Institute), rabbit anti-MafA (1:1000, Betalogics (J&J); #LP9872). The following secondary antibodies were used: goat anti-rabbit immunoglobulin G (IgG) (H+L), Alexa Fluor 594 (1:1000, Life Technologies; #A11037) and goat anti-mouse IgG (H+L), Alexa Fluor 488 (1:1000, Life Technologies; #A11029).

For quantification of islet cellular composition, pancreatic sections were scanned using a Zeiss Axio Scan.Z1 slide scanner at the Louise Pelletier Histology Core (University of Ottawa). For each mouse, all islets present on the slide were analyzed, excluding islets containing < 30 cells. Between 3 and 54 islets per sample were manually quantified from IF images using QuPath v0.5.0

bioimaging analysis software. For each biological replicate, the mean of all islet measurements was used for statistical analysis and represented by the larger data points. In comparison, individual islet values are also shown in the background of each plot as smaller data points. The percentage of insulin-, somatostatin-, and glucagon-positive area was calculated as [(hormone$^+$ area / total islet area) × 100]. The percentage of Ucn3-positive area was calculated as [(Ucn3$^+$ area / insulin$^+$ area) × 100]. The percentage of MafA-positive cells was calculated as [(MafA$^+$ cells / total islet cells) × 100].

2.6 Static GSIS assay

Static GSIS was performed as previously described (95). For these experiments, we used islets isolated from Casp1/11/Ripk3 DKO mice and littermate-derived WT controls. We also used islets isolated from C57BL/6J mice treated with either DMSO (vehicle control) or a combination of the Casp1 and Ripk3 inhibitors Ac-YVAD-cmk (0.5 μM; Cayman Chemical; #10014) and UH15-38 (0.5 μM; Med Chem Express; #HY-158312) for 24 hours. For each replicate, 10 islets from the same mouse were hand-picked into 1.5 mL microcentrifuge tubes with a small volume of RPMI medium (Multicell; #350-000 CL) supplemented with 1% penicillin-streptomycin (Gibco; #15140122) and 10% FBS (Multicell; #090-150). Islets were pelleted by centrifugation at 2000 rpm for 1 minute, and the supernatant was removed. Islets were washed with Krebs-Ringer bicarbonate HEPES buffer (KRBH; 115 mM NaCl, 5 mM KCl, 24 mM NaHCO3, 2.5 mM CaCl2, 1 mM MgCl2, 10 mM HEPES, 0.1% w/v bovine serum albumin (BSA)), followed by a second centrifugation (2000 rpm, 1 minute) and removal of supernatant. A pre-incubation with 500 μL KRBH buffer was added to each tube, and the islets were incubated for 1 hour at 37°C and 5% CO_2, with the lids open. Islets were pelleted and spun, and the supernatant was discarded. Cells

were then placed in 500 µL of low-glucose (2.8 mM) KRBH buffer for 1 hour, followed by 1 hour in 500 µL of high-glucose (16.7 mM) KRBH buffer at 37°C and 5% CO_2. At the end of each incubation, the low- and high-glucose KRBH supernatants were collected and stored at -20°C. To assess total insulin content, 500 µL of acid ethanol (75% EtOH, 1.5% HCl) was added to islet pellets overnight at 4°C. Equal volumes of 1 M Tris-base were added to neutralize the extract, and the mixture was stored at -20°C. Insulin concentrations were measured by ELISA (ALPCO; #80-INSMR-CH10), and somatostatin was measured by enzyme immunoassay (EIA) (Phoenix Pharmaceuticals, Inc.; #FEK-060-03).

2.7 Dynamic GSIS assay

Dynamic GSIS was assessed in islets isolated from DKO mice and littermate-derived WT controls, as well as in islets from C57BL/6J mice treated with either DMSO (vehicle control) or a combination of Ac-YVAD-cmk (100 µM) and GSK'872 (5 µM) for 24 hours. For each replicate, 70 islets from the same mouse were handpicked and loaded into Perspex microcolumns between two layers of acrylamide-based microbeads (Biorep Technologies; PERI-BEADS). Islets were assayed using a Biorep Technologies system and maintained at 37°C with various glucose concentrations diluted in KRBH buffer (115 mM NaCl, 5 mM KCl, 24 mM $NaHCO_3$, 2.5 mM $CaCl_2$, 1 mM $MgCl_2$, 10 mM HEPES, 0.1% w/v BSA. Following a 40 minute pre-incubation period, islets were exposed sequentially with KRBH containing varying glucose concentrations as follows: LG (2.8 mM) for 15 minutes at 40 µL/min; HG (16.7 mM) for 15 minutes at 80 µL/min; HG for 30 minutes at 40 µL/min; LG for 25 minutes at 40 µL/min; KCl (30 mM) for 15 minutes at 80 µL/min; KCl for 20 minutes at 40 µL/min; and finally LG for 25 minutes at 40 µL/min. Perifusate fractions were collected every 2.5 or 5 minutes and maintained at 4°C in round-bottom

96-well plates throughout the experiment. Samples were stored at -20°C short-term until insulin concentrations were quantified by ELISA (ALPCO; #80-INSMR-CH10) and somatostatin was measured by EIA (Phoenix Pharmaceuticals, Inc.; #FEK-060-03).

2.8 Statistical analysis

All statistical analyses were performed using GraphPad Prism (version 10.6, GraphPad Software Inc., La Jolla, CA, USA). Normality of data was determined using the Shapiro-Wilk test ($\alpha = 0.05$). For normally distributed data, differences between groups with a single variable were determined using an unpaired t-test with Welch's correction. For comparisons involving three or more groups, a one-way ANOVA was used, while a two-way ANOVA was applied when analyzing data with two independent variables. For non-normally distributed data, differences between groups were assessed using an unpaired Mann-Whitney U test. Specific statistical tests are indicated in the corresponding figure legends. Statistical significance was defined as $*p < 0.05$, $**p < 0.01$, $***p < 0.001$, and $****p < 0.0001$. Data are presented as mean ± SEM.

Chapter 3: Results

3.1 Characterization of pancreatic cell markers in Casp1/11/Ripk3 DKO islets

3.1.1 Casp1/11/Ripk3 deletion alters islet cell transcriptional markers

Given the clear hypersecretion phenotype observed in LFD DKO mice, we compared islet transcript levels between genotypes. We started by comparing transcripts associated with identity and functional maturity, including *Ins1* and *Ins2*, which encode proinsulin peptides (96), as well as *MafA* and *Nkx6.1*, transcription factors essential for maintaining mature β-cell identity and GSIS (97,98). In addition, we assessed *Ucn3*, a marker of β-cell maturity that regulates local inhibitory

control of insulin secretion (17). Under LFD, only male DKO islet *Ins1* relative expression was increased (Figure 5A). In comparison, HFD DKO islets showed additional transcriptional differences, with significant increases in *Ins1*, *Ins2*, and *Nkx6.1* in males, as well as increased *Ucn3* in male islets (Figure 5C, D).

We next evaluated β-cell transcripts involved in glucose sensing and metabolic function. Relative expression of *Gck*, a key glucose sensor that regulates GSIS (99), was elevated in male DKO islets under both LFD and HFD conditions (Figure 5A, C). In addition, *Slc2a2*, which encodes the glucose transporter GLUT2 responsible for facilitating glucose entry into the β-cell (100), showed increased fold change in HFD DKO islets in both sexes (Figure 5C, D). To determine whether other endocrine cell populations were affected, transcripts beyond the β-cell were also assessed. In the LFD group, no differences were observed in *Crhr2*, the δ-cell receptor responsible for binding Ucn3 (101) (Figure 5A, B). Additionally, glucagon (*Gcg*) and somatostatin (*Sst*) were measured in the HFD group, with no significant differences detected between genotypes (Figure 5C, D).

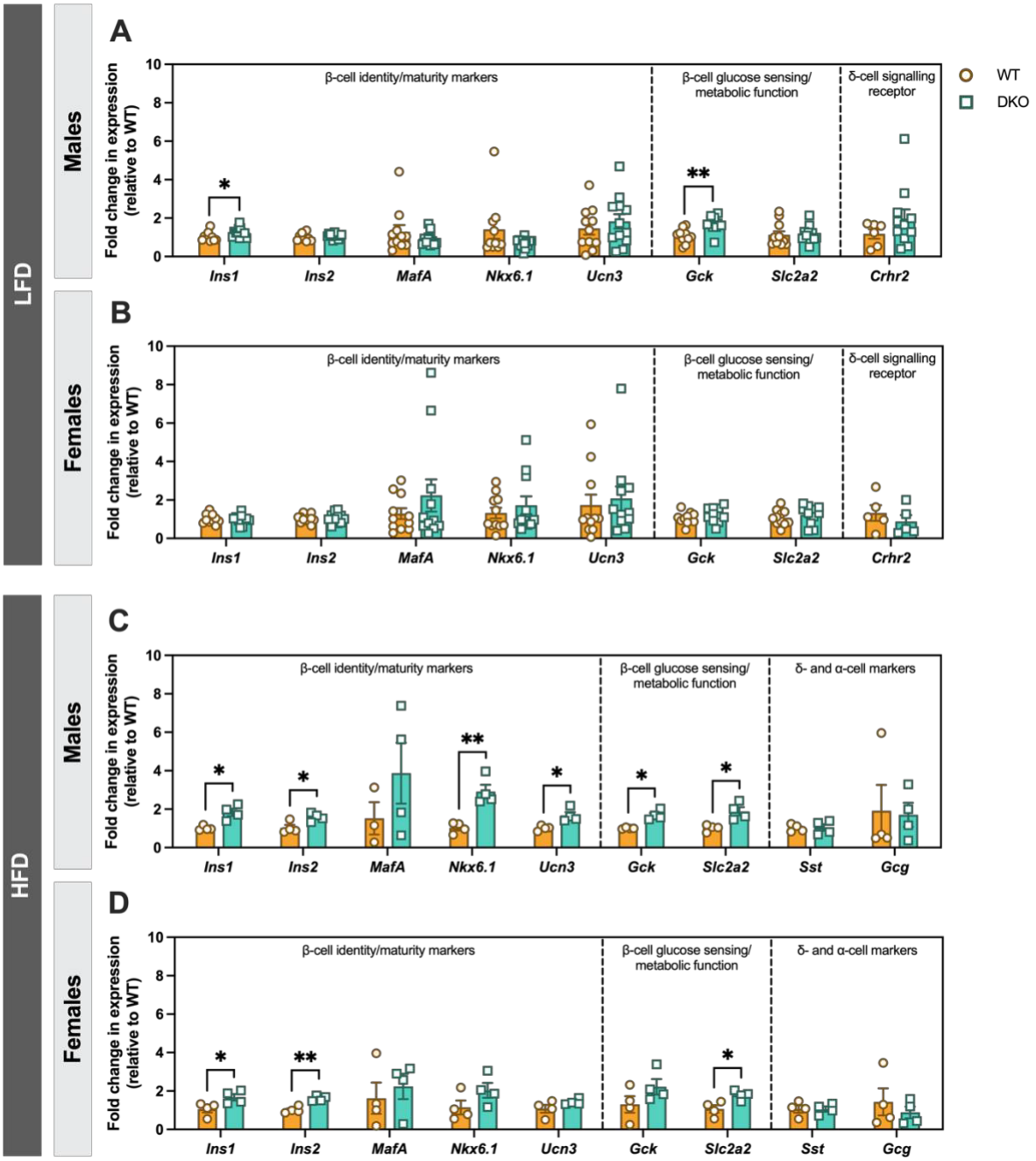

Figure 5. Casp1/11/Ripk3 DKO mice exhibit altered expression of select islet genes.
(A-D) Gene transcripts associated with β-cell identity and maturity (*Ins1*, *Ins2*, *MafA*, *Nkx6.1*, *Ucn3*) and β-cell glucose sensing and metabolic function (*Gck*, *Slc2a2*) were measured in isolated islets from male and female mice maintained on either a LFD or HFD. In addition, δ-cell signalling (*Crhr2*) was assessed in LFD islets **(A-B)**, while δ- and α-cell markers (*Sst*, *Gcg*) were assessed in HFD islets **(C-D)**. Transcript abundance was quantified by RT-qPCR. Data are presented as mean ± SEM (n = 4-12 mice per genotype). Statistical significance was determined using an unpaired two-tailed t-test with Welch's correction. *$p < 0.05$, **$p < 0.01$.

3.1.2 Reduced UCN3-positive cell area in Casp1/11/Ripk3 DKO pancreatic islets

To examine islet cellular composition, paraffin-embedded pancreatic tissue sections from WT and DKO mice were sectioned and analyzed by IF staining for glucagon, UCN3, somatostatin, and MAFA. Each of these stains were co-stained with insulin and the nuclear stain DAPI. We wanted to determine whether the increased insulin secretion observed in LFD-fed DKO mice was associated with changes in endocrine cell composition or overall cell morphology.

Although the average islet size per section was larger relative to WT in some female DKO HFD groups, no consistent genotype-dependent effects on islet size or overall morphology were observed in DKO mice (Figure 6A-B, 7A-G). Islets from HFD-fed mice were generally larger than those from LFD-fed mice across both sexes, supporting the effects of HFD feeding (Figure 7A-G). While the LFD DKO female mice displayed a reduction in glucagon-positive area normalized to represent alpha-cell area, the overall averages of all LFD and HFD groups fell within the anticipated 10-20% expected alpha-cell composition observed in mice (14) (Figure 8A, F, J, N). In LFD conditions, females showed a significant increase in the percentage of insulin-positive area in DKO mice, whereas under HFD conditions, this increase was observed in males. This measure was normalized to total pancreas area and is commonly considered a proxy for relative β-cell area (Figure 8B, G, K, O). The percentage of somatostatin-positive area per islet was decreased in HFD DKO mice, a proxy for δ-cell area (Figure 8C, H, L, P). Interestingly, the percentage of UCN3-positive area normalized to insulin-positive area per islet was reduced in all DKO mice (Figure 8D, I, M, Q). To further assess β-cell maturity, MAFA, a nuclear transcription factor involved in insulin gene expression, was examined. MAFA is expressed in the nuclei of approximately 80% of pancreatic β-cells (~52-64% of all islet cells) (102). While both WT and DKO islets were found to be within this range, no differences were found between the percentage of MAFA-positive

nuclei normalized to the total amount of islet cells (Figure 8E). Overall, the DKO mice appear to exhibit reduced UCN3-positive area, with variable changes in insulin and somatostatin protein.

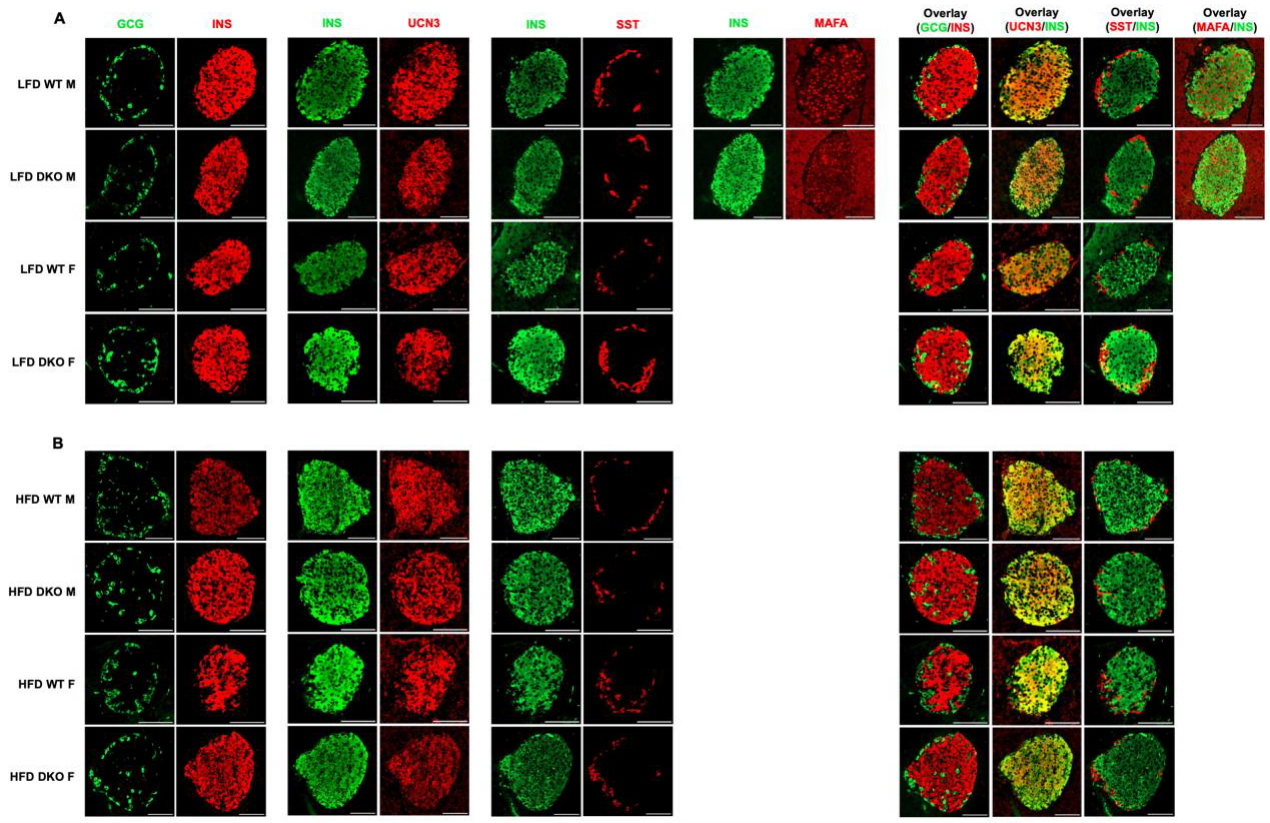

Figure 6. No morphological differences in Casp1/11/Ripk3 DKO islets.
(A-B) Representative IF images of pancreatic islets stained for glucagon (GCG), somatostatin (SST), UCN3, and MAFA, each co-stained with insulin (INS), from mice maintained on either a LFD (A) or HFD (B). Scale bars = 100 μm. Images for each marker are derived from the same representative islet per condition.

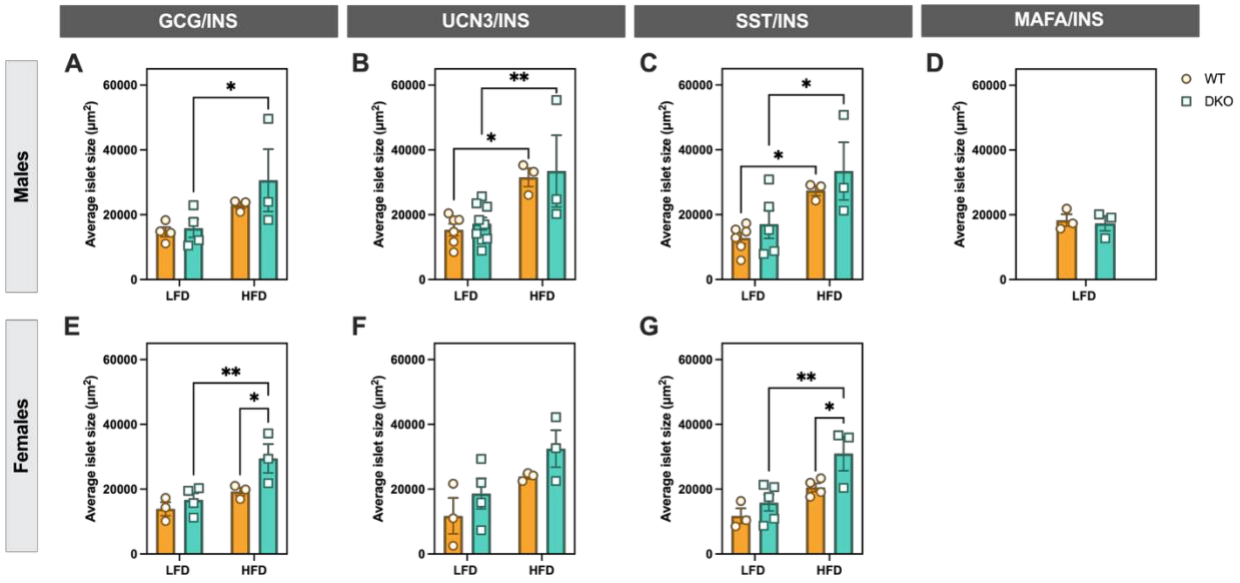

Figure 7. HFD-fed mice exhibit increased average islet size compared with LFD-fed mice. Average islet size was quantified from IF images of pancreatic islets co-stained for glucagon (GCG), UCN3, somatostatin (SST), MAFA, and insulin (INS) from mice maintained on either a LFD or HFD. Data are shown for males **(A-D)** and females **(E-G)**. Values represent mean ± SEM of average islet size per section per mouse (n = 3-9 mice per genotype). Statistical significance was assessed using two-way ANOVA with multiple comparisons correction. *$p < 0.05$, **$p < 0.01$.

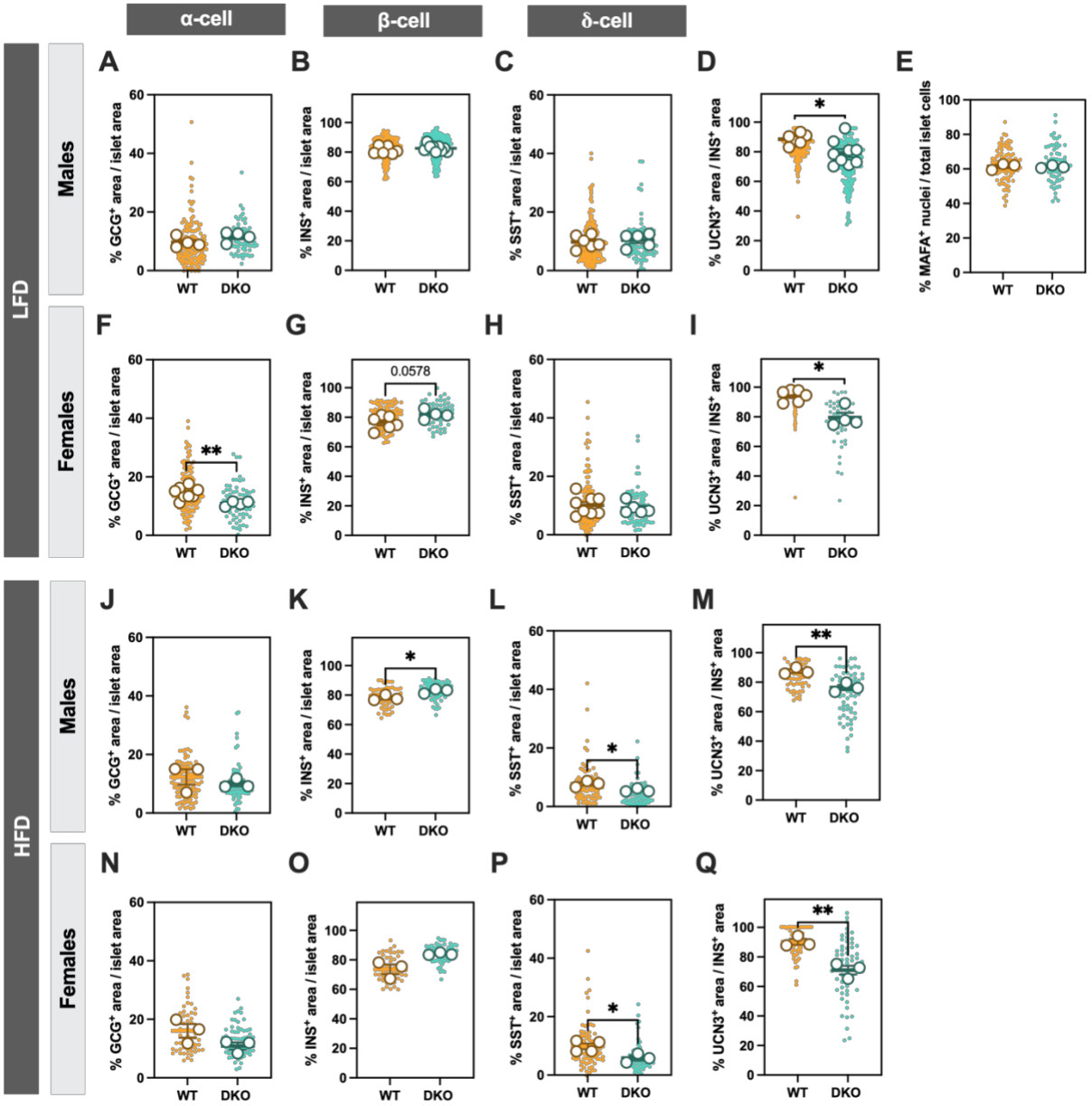

Figure 8. Casp1/11/Ripk3 DKO mice display changes in endocrine cell composition.
Paraffin-embedded pancreatic sections were analyzed by IF staining to quantify selected islet hormones. **(A, F, J, N)** % glucagon (GCG)$^+$ area per islet. **(B, G, K, O)** % insulin (INS)$^+$ area per islet. Representative images from UCN3/INS IF staining are shown. **(C, H, L, P)** % somatostatin (SST)$^+$ area per islet. **(D, I, M, Q)** % UCN3$^+$ area normalized to INS$^+$ area per islet. **(E)** % MAFA$^+$ nuclei per total islet cells. Quantification of GCG$^+$, INS$^+$, and SST$^+$ area was calculated as: (hormone$^+$ area / total islet area) × 100. UCN3$^+$ area was quantified as: (UCN3$^+$ area / INS$^+$ area) × 100. MAFA$^+$ nuclei were quantified as: (MAFA$^+$ nuclei / total islet cells) × 100. Small dots represent individual islets (3-54 per mouse); large dots indicate the mean per mouse (n = 3-9 mice per genotype). Data are mean ± SEM. Statistical significance was assessed using an unpaired, two-tailed Welch's t-test. *$p < 0.05$, **$p < 0.01$.

3.1.3 Measuring somatostatin secretion in response to static GSIS

Relative transcript and protein quantifications suggested potential changes in the UCN3-somatostatin signalling axis in DKO islets. To further investigate this pathway, we measured somatostatin secretion from isolated islets during a static GSIS assay. In response to glucose, β-cells are expected to increase UCN3 release, thereby activating δ-cells and promoting somatostatin secretion (30).

Islets from female WT and DKO mice were incubated for 1 hour under low (2.8 mM) and high (16.7 mM) glucose conditions, and somatostatin levels were quantified in the supernatant. Total insulin content was also assessed from acid-ethanol extracts to confirm islet insulin content. In both WT and DKO islets, glucose stimulation did not increase somatostatin secretion in the supernatant (Figure 9A). In addition, a corresponding insulin secretory response to glucose was not observed in either genotype or were any differences in insulin content (Figure 9B-C), limiting interpretations of the somatostatin secretion data under these conditions.

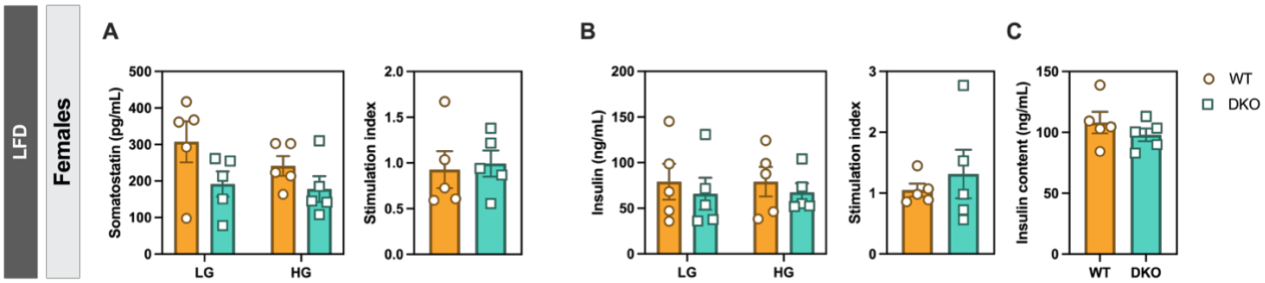

Figure 9. Insulin and somatostatin secretion from Casp1/11/Ripk3 DKO islets in static secretion assay.

(A) Somatostatin secretion from isolated islets of female LFD-fed mice following 1-hour incubations in low glucose (LG; 2.8 mM) and high glucose (HG; 16.7 mM). **(B)** Insulin secretion under corresponding conditions. **(C)** Total insulin content following overnight acid ethanol extraction. The stimulation index was calculated as the ratio of HG to LG secretion. Data are mean ± SEM (n = 5 mice per genotype). Statistical significance was assessed using two-way ANOVA or unpaired, two-tailed Welch's t-test, as appropriate.

3.2 Validation of the metabolic phenotype in Casp1/Ripk3 mice

3.2.1 Metabolic phenotypes are preserved without Casp11 deletion

All mice used in the initial experiments were Casp1/11/Ripk3-deficient, as this genetic model was originally developed for an infection study. Cytosolic LPS primarily activates Casp11 from gram-negative bacteria to trigger inflammation via a programmed form of cell death called pyroptosis (103). Therefore, in the absence of such stimuli, we would not expect Casp11 to contribute significantly to the observed phenotypes in our initial model. To determine whether Casp11 contributed to the observed phenotype, we rederived the mouse line by obtaining new Casp1 KO mice and crossing them with Ripk3 KO mice to generate a Casp1/Ripk3 DKO cohort lacking Casp11 deletion. Under LFD conditions, these mice showed no differences in body weight compared with WT controls (Figure 10A, D). While single KOs of Casp1 and Ripk3 in male mice showed no differences in glucose tolerance, the DKO mice exhibited significantly improved glucose tolerance, suggesting a combined effect of deleting both enzymes (Figure 10B). In DKO females, there was a trend towards improved glucose tolerance, which was not measured in the single KOs (Figure 10E). Similarly to the initial cohort, no changes in insulin sensitivity were observed during ipITT (Figure 10C, F).

To investigate the incretin effect, where oral glucose elicits a greater insulin response than ipGTT, an oral GTT was performed in male mice. This result demonstrated an even more pronounced glucose-tolerant phenotype in DKO mice, reflected by a significant reduction in glucose area under the curve (AUC) compared with WT (Figure 11A).

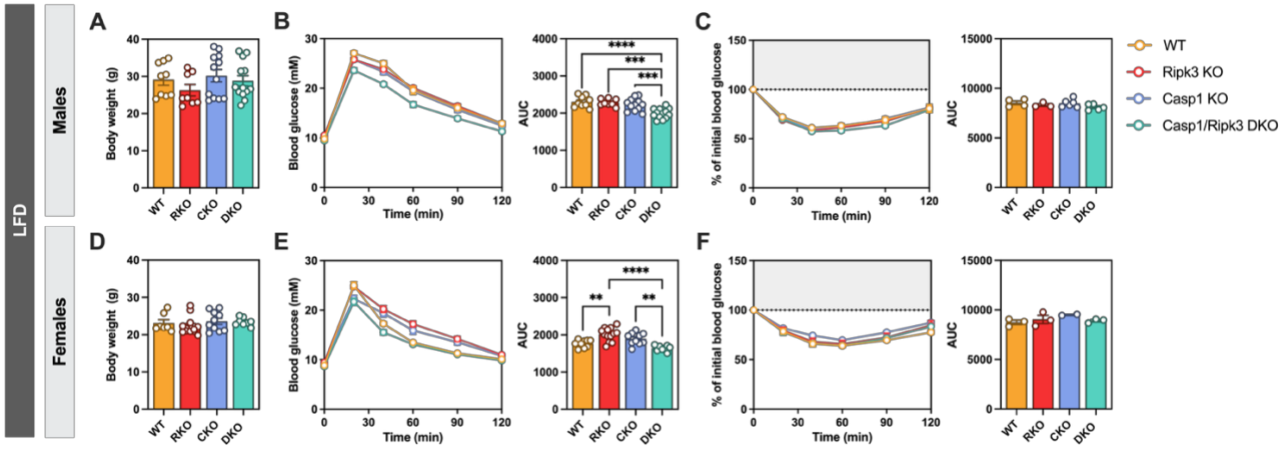

Figure 10. Metabolic phenotypes remain preserved in the absence of Casp11 deletion. **(A, D)** Body weight of WT, Ripk3 KO (RKO), Casp1 KO (CKO), and Casp1/Ripk3 (DKO) male and female mice fed a LFD. **(B, E)** ipGTT (1.5 g/kg glucose in 0.9% saline) was performed on 4.5-hour fasted LFD-fed mice. Blood glucose was measured over 120 minutes. **(C, F)** ipITT (0.5 U/kg insulin) was performed on 4.5-hour fasted LFD-fed mice, with glucose measured over 120 minutes. Data are mean ± SEM (n = 2-13 mice per genotype). Body weight and AUC values for GTT and ITT were analyzed using one-way ANOVA. $^{**}p < 0.01$, $^{***}p < 0.001$, $^{****}p < 0.0001$.

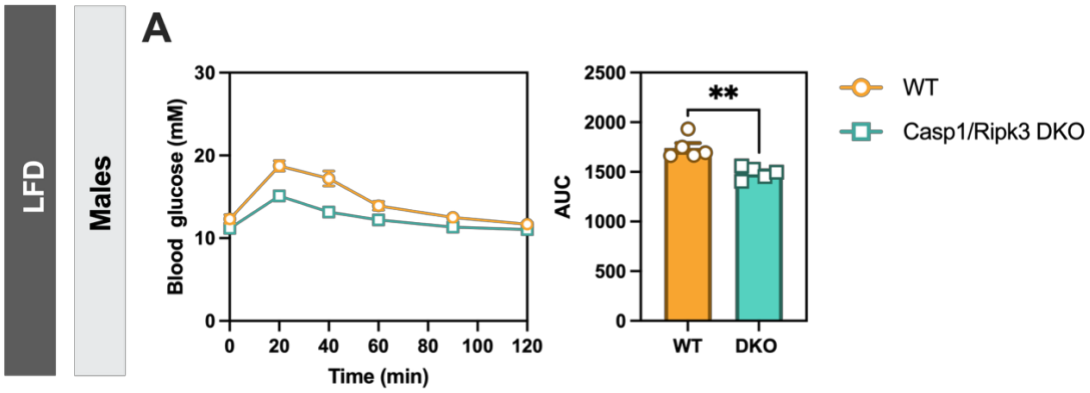

Figure 11. Casp1/Ripk3 DKO mice exhibit improved glucose tolerance during oral glucose tolerance testing.

(A) Oral glucose tolerance test (oGTT; 2 g/kg glucose in 0.9% saline) was performed in LFD-fed mice following a 5-hour fast. Blood glucose was measured over 120 minutes. Data are presented as mean ± SEM (n = 5 mice per genotype). AUC values for the oGTT were calculated and analyzed using an unpaired, two-tailed Welch's t-test. $^{**}p < 0.01$.

3.3 Pharmacological inhibition of Casp1/Ripk3

3.3.1 *In vivo* pharmacological inhibition of Casp1/Ripk3 mimics the genetic phenotype

To better understand the metabolic phenotypes observed in the genetic DKO mice, we next examined whether similar effects could be reproduced through pharmacological inhibition of Casp1 and/or Ripk3. Saline was administered to C57BL/6J male and female mice for two days to establish baseline glucose tolerance, measured by ipGTT. Mice were then injected with a combination of the irreversible Casp1 inhibitor Ac-YVAD-cmk (2.5 mg/kg) and/or the Ripk3 inhibitor GSK'872 (2.5 mg/kg) for two consecutive days, and glucose tolerance was reassessed (Figure 12A). Pharmacological inhibition of Casp1/Ripk3 significantly reduced glucose excursion during the ipGTT, recapitulating the metabolic phenotype observed in the genetic DKO model (Figure 12B). While single-drug inhibitor treatments showed a trend toward reduced ipGTT AUC, the combination of both inhibitors showed an additive effect. Additionally, no differences in insulin sensitivity were found between saline-treated and dual drug-treated male mice (Figure 12C).

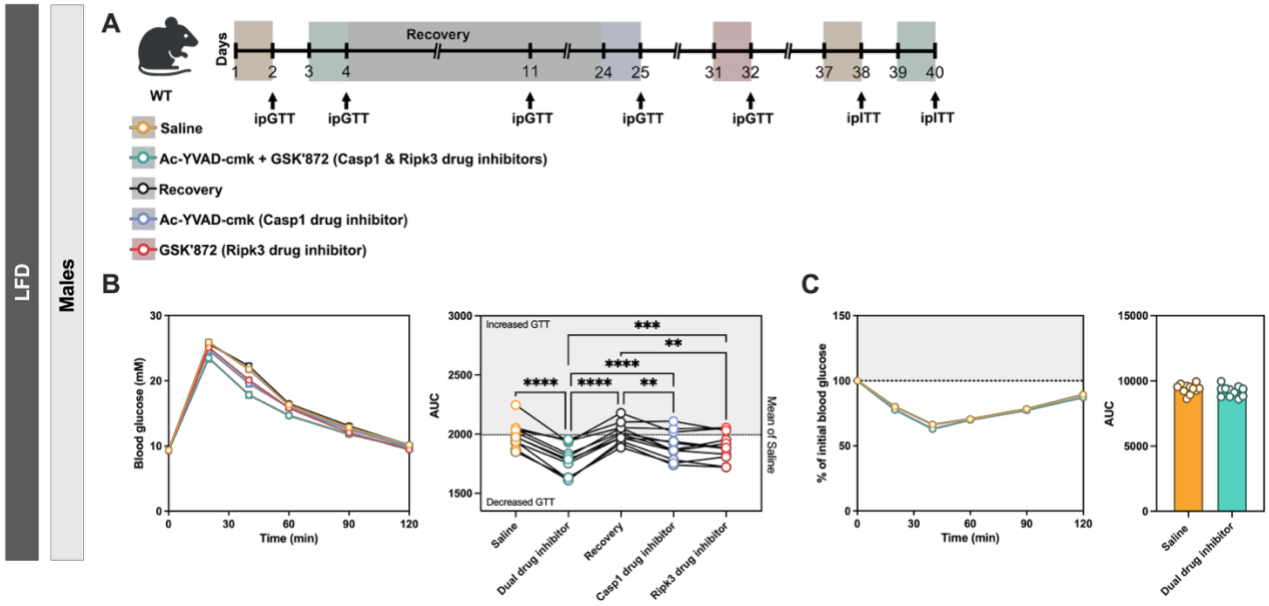

Figure 12. *In vivo* pharmacological inhibition of Casp1/Ripk3 mimics the genetic phenotype.

(A) Experimental timeline for male C57BL/6J mice over 40 days. Mice received ip injections of saline or Casp1/Ripk3 inhibitors (Ac-YVAD-cmk and GSK'872; 2.5 mg/kg in 0.9% saline) over 24 hours (two injections total). **(B)** Ip GTTs (2 g/kg glucose in 0.9% saline) were performed following a 4.5 h fast, with blood glucose measured over 120 minutes. **(C)** Ip ITTs (0.6 U/kg insulin) were performed in 4.5 h-fasted LFD-fed mice, with blood glucose measured over 120 minutes. Data are presented as mean ± SEM (n = 11 mice per condition). Statistical significance was determined using repeated-measures one-way ANOVA for (B) and an unpaired, two-tailed Welch's t-test for (C). $^{**}p < 0.01$, $^{***}p < 0.001$, $^{****}p < 0.0001$.

3.3.2 Casp1/Ripk3 inhibition enhances insulin secretion while somatostatin release remains unchanged

Looking to determine whether the genetic phenotype could be reproduced *ex vivo*, isolated islets from male C57BL/6J mice were treated with DMSO (vehicle control) or a combination of Z-YVAD-fmk (100 μM) and GSK'872 (5 μM) for 24 hours, followed by dynamic assessment of GSIS by perifusion. Islets treated with Casp1 and Ripk3 inhibitors secreted more insulin in response to glucose than vehicle controls (Figure 13A). Interestingly, KCl-induced insulin release remained unchanged between the two groups (Figure 13A). Overall, these results demonstrate that the genetic insulin hypersecretion phenotype can be replicated using acute pharmacological inhibitors in islets themselves.

In a second attempt to measure somatostatin secretion from islets, somatostatin levels were quantified using EIA. Although glucose-stimulated somatostatin secretion was detected, no differences in concentration were measured between the two groups (Figure 13B). Similarly, KCl-stimulated somatostatin secretion remained unchanged (Figure 13C).

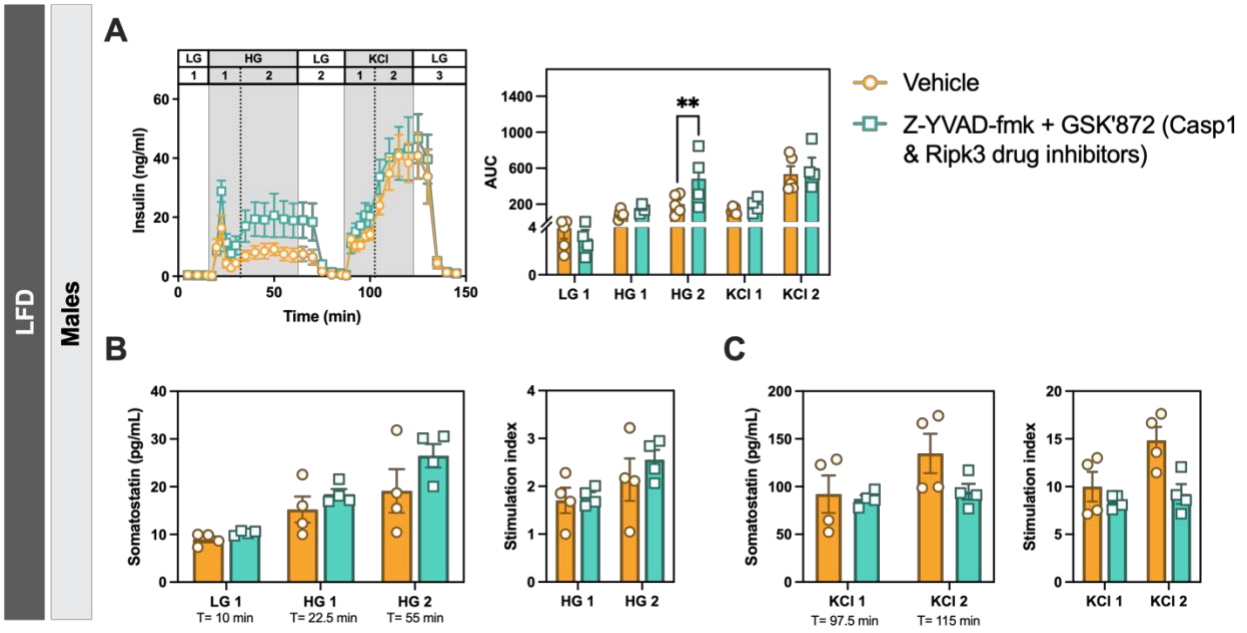

Figure 13. Casp1/Ripk3 inhibition enhances insulin secretion in islets.
(A) Dynamic insulin secretion from isolated islets of C57BL/6J male mice treated with either DMSO (vehicle control) or a combination of the Casp1/Ripk3 inhibitors Z-YVAD-fmk (100 µM) and GSK'872 (5 µM) for 24 hours in response to low glucose (LG; 2.8 mM), high glucose (HG; 16.7 mM), and depolarizing potassium chloride (KCl; 30 mM). Insulin secretion was measured over a 150-minute perifusion period. Perifusion flow rates were as follows: LG 1-3, 40 µL/min; HG 1, 80 µL/min; HG 2, 40 µL/min; KCl 1, 80 µL/min; and KCl 2, 40 µL/min. **(B)** Somatostatin secretion was measured during perifusion under LG 1 (T= 10 minutes), HG 1 (T= 22.5 minutes), and HG 2 (T= 55 minutes) conditions. **(C)** Somatostatin secretion was measured during perifusion under KCl 1 (T= 97.5 minutes) and KCl 2 (T= 115 minutes) conditions. The stimulation index was calculated as HG/LG secretion or KCl/LG secretion. Data are presented as mean ± SEM (n = 4-5 mice per condition). Statistical significance was determined using two-way ANOVA. $^{**}p < 0.01$.

3.4 Effects of exogenous UCN3 and somatostatin on glucose regulation

3.4.1 Blunted UCN3 response following Casp1/Ripk3 DKO

Since fewer UCN3-positive β-cells were observed in pancreatic sections from DKO mice, we aimed to determine whether altered glucose tolerance was associated with decreased UCN3 secretion. To test this, we assessed whether exogenous UCN3 administration prior to an ipGTT could activate inhibitory signalling in β-cells and normalize glucose tolerance in DKO mice. We injected exogenous UCN3 (10 nmol/kg) into male WT and DKO mice 5 minutes before an ipGTT. Exogenous UCN3 caused a pronounced increase in blood glucose in WT mice, while DKO mice displayed a substantially smaller relative change (Figure 14A). This blunted response in DKO mice persisted even at a 5-fold higher dose.

3.4.2 Glucose tolerance in Casp1/Ripk3 DKO following octreotide administration

Given potential alterations in the β-δ signalling axis, we next performed a similar experiment using the somatostatin analog octreotide. This time, mice were injected 30 minutes before an ipGTT. As expected, WT mice injected with octreotide showed a spiking glucose curve compared with their saline controls (Figure 15A-B). Interestingly, unlike in the previous experiment, the blunted response observed in DKO mice was no longer evident following octreotide treatment, with a relative change comparable to that in WT.

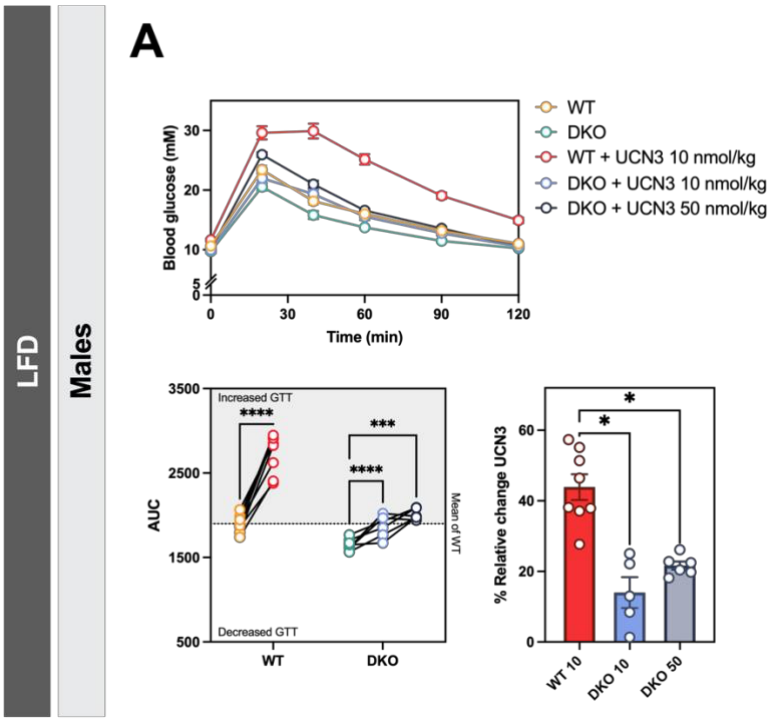

Figure 14. Blunted UCN3 response during GTT in Casp1/Ripk3 DKO mice.
(A) Following a 4.5-hour fast, male WT and DKO mice received ip injections of saline or exogenous UCN3 (10 or 50 nmol/kg) 5 minutes prior to an ip GTT (2 g/kg glucose in 0.9% saline). Paired AUC values were calculated for all conditions, and the percent relative change in response to UCN3 was calculated as [(UCN3 AUC - saline AUC) / saline AUC × 100]. Data are presented as mean ± SEM (n = 5-8 mice per condition). Statistical significance was determined using repeated-measures one- or two-way ANOVA, as appropriate. *$p < 0.05$, ***$p < 0.001$, ****$p < 0.0001$.

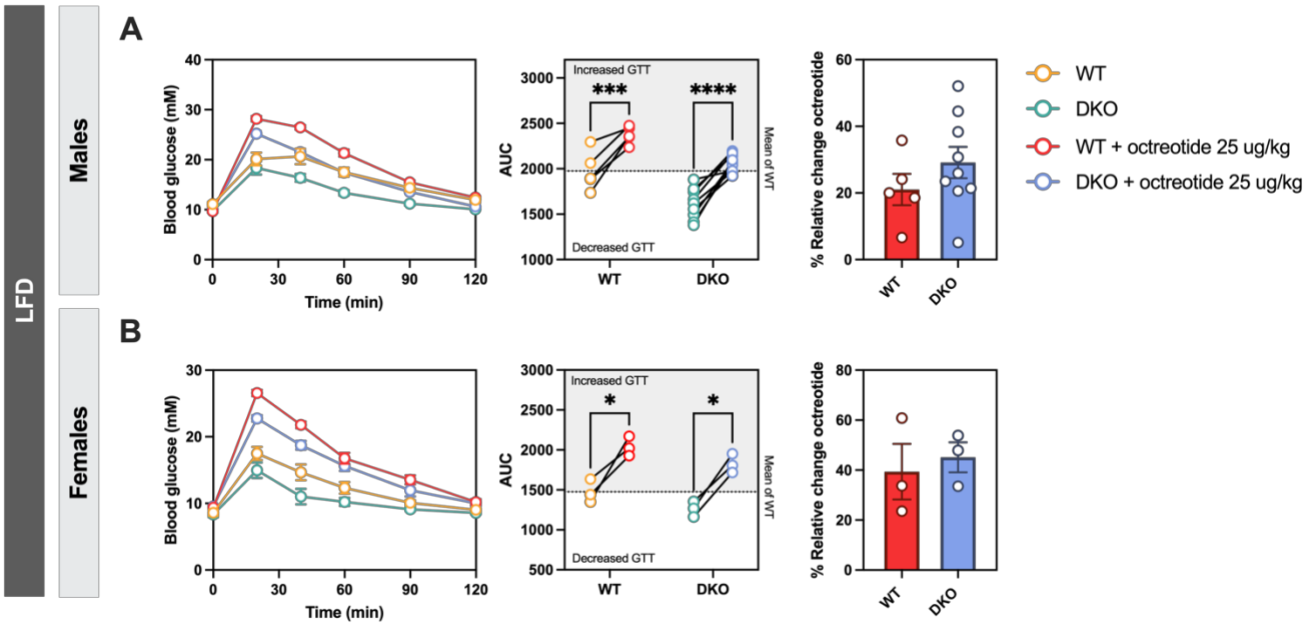

Figure 15. No changes in octreotide response during GTT.
(A-B) Following a 4.5-hour fast, male and female WT and DKO mice received ip injections of saline or the somatostatin analogue octreotide (25 µg/kg) 30 minutes prior to an ip GTT (2 g/kg glucose in 0.9% saline). Paired AUC values were calculated for all conditions, and the percent relative change in response to octreotide was calculated as [(octreotide AUC - saline AUC) / saline AUC × 100]. Data are presented as mean ± SEM (n = 3-9 mice per condition). Statistical significance was determined using repeated-measures two-way ANOVA or a two-tailed Welch's t-test, as appropriate. *$p < 0.05$, ***$p < 0.001$, ****$p < 0.0001$.

Chapter 4: Discussion

Casp1 and Ripk3 are best known for their roles in inflammatory signalling and regulated cell death, but more recent work suggests they may also contribute to metabolic regulation beyond these classical functions. In this study, combined deletion of Casp1 and Ripk3 in LFD-fed mice consistently improved glucose tolerance and enhanced insulin secretion, leading us to investigate whether changes in intra-islet signalling could underlie this phenotype.

4.1 Casp1/Ripk3 signalling and islet hormone regulation

4.1.1 Role of intra-islet paracrine signalling

While β-cells possess specialized machinery to synthesize, store, and secrete insulin in a regulated manner, optimal glycemic regulation depends on communication among multiple cell types and tissues (104,105). More specifically, in literature, it has been found that glucagon secreted by α-cells enhances GSIS by binding to the glucagon receptor and, at higher concentrations, to the glucagon-like peptide-1 receptor (GLP-1R) on β-cells (106,107). We also know that UCN3 released by β-cells triggers somatostatin-dependent negative feedback that inhibits both β- and α-cells, thereby restoring homeostatic plasma levels (insulin inhibition) (16,98). Taken together, these findings reinforce the notion that insulin release can be altered by hormones such as glucagon, UCN3, and somatostatin. Given that lean DKO mice exhibited increased insulin secretion, we investigated potential alterations in paracrine hormone balance that may contribute to this phenotype.

The increased relative transcript levels of *Ins1* and *Gck* in male LFD DKO mice suggest altered β-cell glucose sensing and insulin gene expression (Figure 5A). However, this increase was not observed in female mice, suggesting that further experiments to assess the functional activity

of β-cell insulin secretion capacity would be required. Following HFD feeding, DKO islets had increased transcript of several β-cell identity and maturity markers. In parallel, genes involved in glucose sensing and metabolic function were also upregulated (Figure 5C-D). However, despite these transcriptional changes, HFD DKO mice previously demonstrated impaired glucose tolerance relative to WT. Ultimately suggesting that the upregulation of β-cell maturity and metabolic genes may represent a maladaptive compensatory response to metabolic stress that is insufficient to maintain glycemic control in the absence of Casp1/11/Ripk3 signalling. This pattern is consistent with previous studies showing that β-cells can initially mount a compensatory response to metabolic stress, leading to increased insulin biosynthesis and glucose-sensing capacity (108,109).

The IF analysis of pancreatic sections from WT and DKO mice reflects islet composition under basal conditions, as mice were not subjected to an acute glucose challenge. MAFA, a critical transcription factor regulating insulin gene expression and GSIS in β-cells (110), showed no difference between male LFD genotypes, suggesting that core β-cell identity is preserved in DKO mice. Interestingly, all DKO islet samples showed a clear reduction in UCN3-positive cells, a marker of β-cell maturity (Figure 8C, H, L, P), without accompanying changes in δ-cell area. Collectively, these findings are consistent with a shift toward a less mature β-cell state that may alter islet paracrine signalling.

Some DKO pancreatic replicate sections from LFD-fed female mice showed significant or trending increases in relative β-cell area, quantified as the percentage of insulin-positive area (Supplemental Figure 1E-G). Although this could reflect a true sex-dependent difference seen in the female DKO mice, all the average measured beta-cell percentages are found to be within the expected beta-cell composition of 65-80% in mice, confounding any definitive conclusions (14).

In contrast, the LFD male cohort showed no difference in β-cell area, with values averaging approximately 80% for both genotypes (Supplemental Figure 1A-D).

δ-cells are strongly activated by paracrine signals, such as UCN3 and GABA, resulting in somatostatin release (16). During a static GSIS, DKO islets showed a trend toward reduced somatostatin release under high glucose compared with WT; however, the absence of a clear glucose-stimulated response across genotypes limits the interpretation of these findings (Figure 9A-C). This result rather reflects the technical limitations of the static GSIS assay, since there was an overall lack of insulin response to high glucose. Somatostatin secretion was assessed again in the supernatant of islets treated acutely with Casp1/Ripk3 inhibitors during dynamic GSIS. High glucose increased somatostatin secretion approximately twofold, but we detected no differences between control and dual-inhibited islets (Figure 13B). While reduced somatostatin-mediated β-cell inhibition could have explained the increased insulin secretion observed in LFD-fed DKO mice, these results are not supportive of this. Together, these findings demonstrate the need to further investigate β- and δ-cell signalling crosstalk to better understand the mechanisms underlying the DKO phenotype.

4.1.2 Glucose tolerance independent of Casp11

Within the caspase family, members are traditionally categorized as either apoptotic (Casp2, 3, 6, 7, 8, 9, and 10) or inflammatory (Casp1, 4, 5, 11), each with distinct substrate specificities and roles in various diseases (111). In mice, Casp11 functions as an intracellular sensor for gram-negative bacterial LPS, triggering a form of inflammatory cell death called pyroptosis, which indirectly promotes the release of IL-1β and IL-18 (112,113). In humans, the Casp11 gene is split into Casp4 and Casp5, both of which are considered functional orthologs of murine Casp11 (114). While this project did not involve infection or exposure to gram-negative bacteria, so no catalytic

activity from this caspase would be expected, the initial mouse model we used was deficient in Casp11, Casp1, and Ripk3. Therefore, we sought to confirm that the glucose-tolerant, insulin hypersecretion phenotype was not driven by Casp11 deletion in these mice.

Consistent with earlier findings, Casp1/Ripk3 DKO mice did not exhibit increased weight gain under LFD conditions (Figure 10A, D), in line with previous studies showing that single Casp1 or Ripk3 KO mice also do not display altered weight gain (53,115). In male mice, glucose tolerance was significantly increased only in the DKO group, showing a combined requirement for Casp1 and Ripk3 (Figure 10B). This phenomenon suggests a potential additive or synergistic interaction between these pathways that may operate even under non-inflammatory LFD-fed conditions, a concept that has not been previously reported. In DKO female mice, glucose tolerance was not significantly different from that in WT mice. However, a trend toward reduced GTT AUC was observed, which was not present in either single KO (Figure 10E), indicating a more modest or variable effect in female mice. More female mice should be assessed to increase confidence in whether this is a phenotype that affects both sexes in this new Casp1/Ripk3 model. Overall, this strengthens confidence in the reproducibility of this phenotype attributable to the lack of Casp1 and Ripk3.

4.1.3 Acute pharmacological inhibition of Casp1/Ripk3

The use of a whole-body Casp1/Ripk3 DKO mouse model generated from birth helps rule out overt developmental abnormalities. However, acute pharmacological inhibition remains important, as it allows distinction between immediate signalling effects and potential compensatory adaptations that may develop over time in the genetic model. Combined pharmacological inhibition of Casp1 and Ripk3 (Ac-YVAD-cmk and GSK’872) in male LFD WT

mice was associated with improved glucose tolerance (Figure 12B). In contrast, inhibition of either pathway alone was insufficient to produce this effect. Interestingly, when we stopped administering both drugs, glucose tolerance returned to baseline, indicating that the metabolic effects of Casp1/Ripk3 inhibition are reversible and depend on continued pathway suppression. To date, no studies have directly examined Casp1 or Ripk3 inhibition under LFD conditions. However, individual Casp1 inhibition or broader necroptosis inhibition has been shown to facilitate metabolic benefits under conditions of metabolic stress (66,116). Additionally, the lack of differences in insulin sensitivity between conditions further supports a role for Casp1/Ripk3 in regulating insulin secretion rather than peripheral insulin action (Figure 12C). Overall, this suggests that the Casp1/Ripk3 inhibition/deletion phenotype can be induced acutely without requiring long-term systemic metabolic or cellular reprogramming.

Another acute inhibition experiment was performed using the Casp1/Ripk3 inhibitors Z-YVAD-fmk and GSK'872 on isolated islets from WT LFD-fed mice during perifusion to assess GSIS. After 24 hours of treatment, islets exposed to the inhibitors secreted more insulin in response to glucose compared with untreated controls (Figure 13A). Interestingly, no differences in insulin secretion were observed when islets were exposed to the depolarizing agent KCl. In this context, high concentrations of KCl directly depolarize the β-cell plasma membrane, effectively bypassing upstream glucose-sensing mechanisms and forcing robust insulin secretion. Since KCl bypasses glucose sensing and directly induces membrane depolarization, the unchanged response suggests that Casp1/Ripk3 inhibition enhances upstream glucose-dependent signalling rather than the insulin exocytosis machinery itself. However, this interpretation is further complicated by the genetic model, where DKO islets displayed increased insulin secretion in response to KCl during perifusion (Figure 4B, D). These opposing results between acute pharmacological inhibition and

chronic genetic deletion could indicate that a long-term loss of Casp1 and Ripk3 could alter β-cell insulin content, calcium handling, or the exocytotic machinery in ways not observed in short-term inhibitor experiments.

4.1.4 Altered responses to exogenous UCN3 and somatostatin analog

As previously mentioned, UCN3 and somatostatin are important hormones in regulating glucose homeostasis. An important finding by van der Meulen et al. (2015) found that in response to glucose, secreted UCN3 from the β-cell binds to CRHR2α receptors on the δ-cell, triggering somatostatin release (16). This paracrine signalling loop provides negative feedback on insulin secretion, thereby regulating glucose tolerance. In the same study, they found that when mice were administered additional UCN3 prior to GTT, plasma insulin levels decreased and glucose tolerance worsened (16).

Inspired by their findings, we repeated this experiment in our DKO mice and found that exogenous UCN3 administration reduced glucose tolerance. However, the magnitude of the response was clearly blunted, as the relative change in GTT AUC induced by UCN3 was significantly lower in DKO mice than in WT controls (Figure 14A). Interestingly, increasing the UCN3 peptide concentration five-fold in DKO mice still resulted in only a modest increase in the relative change, further confirming that the reduced responsiveness is not due to a lack of UCN3 peptide availability (we could not increase the dose in WT mice as they were already reaching the maximum blood glucose measurement on the hand-held glucometer; ~33 mM). In contrast, when the experiment was repeated in the presence of the somatostatin analog octreotide, the blunted insulin response in DKO mice was no longer observed (Figure 15A-B). As somatostatin-induced β-cell inhibition appears to be preserved, these findings suggest that the loss of Casp1/Ripk3 may

affect signalling upstream, either at the level of CRHR2α-mediated δ-cell activation or within the δ-cell somatostatin release machinery. However, direct measurements of somatostatin secretion were limited in this study and require further investigation from dynamic GSIS assays.

4.2 Sex and diet-dependent effects on metabolic phenotypes

Throughout this project, we intentionally analyzed male and female mice separately, given well-established sex differences in glucose metabolism, insulin sensitivity, and susceptibility to metabolic disease (117–119). For example, female mice typically exhibit lower blood glucose levels and improved glucose clearance during GTTs compared with males (120). In the early stages of this study, many metabolic phenotypes observed in the Casp1/11Ripk3 DKO model were broadly consistent across sexes, including body weight, glucose tolerance, insulin sensitivity, and insulin secretion.

To induce metabolic stress, a HFD was introduced to better model diet-induced obesity and insulin resistance. However, previous work from this project indicated that HFD feeding appears to overwhelm the underlying DKO phenotype, such that the enhanced GSIS observed under LFD conditions is largely lost. This is likely because prolonged HFD exposure induces a strong state of insulin resistance that can mask or override more subtle alterations in intra-islet signalling pathways. Overall, the pathway(s) affected by Casp1/Ripk3 deficiency may be more relevant under physiological or mildly stressed conditions rather than severe metabolic overload.

Interestingly, when assessing endocrine cell composition, both LFD and HFD male and female mice exhibited a reduced UCN3-positive islet area. As expected, HFD feeding increased mean islet size compared with LFD across genotypes (Figure 7), consistent with compensatory islet hypertrophy in response to metabolic stress (121–123). No clear changes were observed in

the percentage of hormone-positive areas within WT female islets across diets compared with males (Figure 8). Within the new Casp1/Ripk3 cohort, female DKO mice appeared more resistant to diet-induced alterations in glucose tolerance, although a clear trend toward improved glucose clearance remained evident (Figure 10E). Together, these findings suggest a degree of sex-dependent resilience in the metabolic response to Casp1/Ripk3 deletion.

4.6 Limitations and considerations of the study

While this project demonstrates that Casp1 and Ripk3 may play a greater role in glucose homeostasis than previously appreciated, several limitations warrant consideration when interpreting these findings. To determine whether the observed changes in glucose metabolism were driven specifically by β-cells or instead reflected altered paracrine signalling within the islet, we aimed to use the immortalized rat insulinoma-derived β-cell line INS1 832/3, which retains glucose responsiveness (124). However, during culturing of this cell line, we encountered multiple technical challenges, including poor cell adhesion and strong sensitivity to Casp1/Ripk3 inhibitors. Importantly, vehicle-treated control cells failed to exhibit an insulin-stimulated response to high glucose, rendering interpretation of treatment effects impossible (Supplemental Figure 2A). Under normal conditions, INS1 832/3 cells should display a stimulation index of at least 2 in vehicle-treated controls (95). The absence of GSIS may have resulted from poor cell adherence, leading to cell loss during supernatant collection in the low-glucose condition and reducing the number of cells available to respond during subsequent HG stimulation. To fix this, we coated plates with collagen and used low-passage (passage 3) cells. However, these modifications did not improve glucose responsiveness. This remains an important consideration, as the findings in this study may reflect contributions from β-cell-specific effects and/or from multiple islet cell types.

While establishing efficient techniques to obtain high islet isolation yields required several months of optimization, a major limitation of this project was the inability to obtain reliable results using static GSIS in mouse islets. Despite repeated attempts, the isolated islets did not consistently respond to basal low-glucose stimulation followed by high-glucose stimulation (Supplemental Figure 3A-D), limiting our ability to interpret insulin secretion using this approach confidently. Later, we learned that other laboratories had also encountered similar challenges with static GSIS during fixed collection times. To address this, we transitioned to measuring GSIS using a dynamic perifusion system. Unlike static GSIS, the perifusion system allows collection of fractions every few minutes, enabling assessment of insulin secretion in a more physiologically relevant manner rather than at a single endpoint. Although this approach required increased coordination between labs, it ultimately strengthened the project by providing a more sensitive assessment of islet function.

Another limitation during this project was our inability to measure different hormonal outputs in islets during GSIS. Unfortunately, we were unable to obtain reliable somatostatin measurements from the static GSIS in DKO mice (Figure 9). This was not entirely surprising, since somatostatin is found in extremely small quantities and is rapidly degraded (125). Similarly, we were unable to directly measure UCN3 in perifusion samples. To our knowledge, measuring UCN3 directly from perifusion samples is not widely reported in the literature. UCN3 is approximately 1000-fold lower in concentration than insulin, making it incredibly difficult to measure. Therefore, insulin was our primary measurable output, making it difficult to draw definitive conclusions regarding the contributions of other endocrine cell types. Consequently, any possible interpretations of UCN3 and somatostatin responses to glucose are largely based on how we understand their paracrine signalling from the literature.

4.7 Research significance and future directions

Consistently throughout this project, inhibition or deletion of Casp1 and Ripk3 resulted in improved glucose tolerance and increased insulin secretion. These findings suggest a previously unrecognized role for inflammatory and cell death pathways. At face value, this phenotype could indicate that diminishing Casp1/Ripk3 signalling diminishes β-cell inhibition and may help counteract hyperglycemia, which could be beneficial in an islet transplantation context, where enhanced insulin secretion may improve diabetic outcomes. However, it remains unclear whether this effect is metabolically beneficial in the long term. More specifically, this apparent protective phenotype was refuted under metabolic stress during HFD feeding, complicating interpretations of its physiological relevance. As such, it is difficult to predict how inhibition of these pathways would perform in a therapeutic setting. Additionally, this could indicate that the DKO islets may be maladaptive, secreting excess insulin even when not strictly required. While this may transiently improve glucose tolerance, it could place additional demand on β-cells and potentially contribute to long-term dysfunction.

DKO mice exhibited clear changes in endocrine cell composition, including a reduction in UCN3-positive area under both LFD and HFD conditions. This may reflect a weakening of the inhibitory paracrine signalling loop. Alternatively, the exogenous UCN3 experiment suggests that alterations in δ-cell somatostatin production may underlie the observed phenotype. To better understand this model, future studies will measure somatostatin secretion in the supernatant of genetic DKO islets during GSIS experiments.

While measuring UCN3 or somatostatin directly during GSIS experiments has been challenging, somatostatin secretion also inhibits α-cell activity and suppresses glucagon release (126). As a next-step experiment, measuring baseline, fasted glucagon levels could help indirectly

answer our questions about somatostatin secretion. In addition, another, more technically challenging approach would be to examine changes in ion channel activity, membrane potential, and exocytosis using patch-clamp electrophysiology better to understand the insulin hypersecretion phenotype in DKO islets.

4.8 Conclusion

Inflammation and cell death are both heavily associated with the development of obesity and T2D. Although we previously found that, in LFD-fed mice, Casp1/11/Ripk3 DKO mice are more glucose-tolerant and secrete more insulin than WT controls. Therefore, the goal of this project was to investigate the mechanisms underlying this phenotype. To summarize, we observed only a few changes in select islet genes, while DKO islets showed a reduction in the percentage of UCN3-positive area, representing a promising finding. We validated the original metabolic phenotypes in the absence of Casp11 deletion, confirming that these effects are specific to Casp1/Ripk3 deletion. We also determined that pharmacological inhibition of Casp1/Ripk3 in both mice and islets produced results like those in the genetic model. Finally, administration of exogenous UCN3 indicated a blunted UCN3 response in DKO mice, an effect not observed with the addition of the somatostatin analogue octreotide. Together, these findings point toward a potential alteration in UCN3-somatostatin signalling as a contributing mechanism. Broadening our mechanistic understanding of how Casp1 and Ripk3 together regulate islet function.

References

1. Sapra A BP. Diabetes. [Updated 2023 Jun 21]. In: StatPearls [Internet]. Treasure Island (FL): StatPearls Publishing; 2024 Jan-. Available from: https://www.ncbi.nlm.nih.gov/books/NBK551501/.
2. Public Health Agency of Canada. Public Health Agency of Canada. 2011. Diabetes in Canada: Facts and figures from a public health perspective [Internet]. Available from: http://www.canada.ca/en/public-health/services/publications/diseases-conditions/diabetes-canada-facts-figures-a-public-health-perspective.html.
3. Diabetes Canada. Gestational diabetes [Internet]. [cited 2026 Mar 22]. Available from: https://www.diabetes.ca/about-diabetes/gestational
4. Lucier J, Weinstock RS. Type 1 Diabetes. [Updated 2023 Mar 3]. In: StatPearls [Internet]. Treasure Island (FL): StatPearls Publishing; 2024 Jan-. Available from: https://www.ncbi.nlm.nih.gov/books/NBK507713/.
5. National Institute of Diabetes and Digestive and Kidney Diseases (NIDDK). https://www.niddk.nih.gov/health-information/diabetes/overview/what-is-diabetes/type-2-diabetes. 2027. Type 2 Diabetes.
6. Diabetes Canada. Diabetes in Canada [Internet]. [cited 2026 Mar 23]. Available from: https://www.diabetes.ca/advocacy-policies/advocacy-reports/national-and-provincial-backgrounders/diabetes-in-canada#:~:text=Among%20people%20in%20Canada%20(1):%2030%25%20live,of%20undiagnosed%20type%202%20diabetes%20are%20included.
7. Diabetes Canada. Type 2 complications [Internet]. [cited 2026 Mar 22]. Available from: https://www.diabetes.ca/about-diabetes/type-2/complications#:~:text=Heart%20disease%20&%20stroke,associated%20with%20type%202%20diabetes
8. Chatterjee S, Khunti K, Davies MJ. Type 2 diabetes. The Lancet. 2017 Jun;389(10085):2239–51. doi:10.1016/S0140-6736(17)30058-2
9. Canadian Chronic Disease Surveillance System (CCDSS). Public Health Agency of Canada. Available from: https://health-infobase.canada.ca/ccdss/data-tool/Index?G=00&V=1&M=4&Y=2017.
10. Hu C, Chen Y, Yin X, Xu R, Yin C, Wang C, et al. Pancreatic endocrine and exocrine signaling and crosstalk in physiological and pathological status. Signal Transduct Target Ther. 2025 Feb 14;10(1):39. doi:10.1038/s41392-024-02098-3
11. Shahid Z, Singh G. Physiology, Islets of Langerhans. 2026. PubMed PMID: 31194442.
12. Da Silva Xavier G. The Cells of the Islets of Langerhans. J Clin Med. 2018 Mar 12;7(3). doi:10.3390/jcm7030054 PubMed PMID: 29534517.
13. Félix-Martínez GJ, Godínez-Fernández JR. Comparative analysis of reconstructed architectures from mice and human islets. Islets. 2022 Jan 1;14(1):23–35. doi:10.1080/19382014.2021.1987827 PubMed PMID: 34689719.
14. Campbell JE, Newgard CB. Mechanisms controlling pancreatic islet cell function in insulin secretion. Nat Rev Mol Cell Biol. 2021 Feb 4;22(2):142–58. doi:10.1038/s41580-020-00317-7
15. Rodriguez-Diaz R, Tamayo A, Hara M, Caicedo A. The Local Paracrine Actions of the Pancreatic α-Cell. Diabetes. 2020 Apr;69(4):550–8. doi:10.2337/dbi19-0002 PubMed PMID: 31882565.

16. van der Meulen T, Donaldson CJ, Cáceres E, Hunter AE, Cowing-Zitron C, Pound LD, et al. Urocortin3 mediates somatostatin-dependent negative feedback control of insulin secretion. Nat Med. 2015 Jul 15;21(7):769–76. doi:10.1038/nm.3872
17. Li C, Chen P, Vaughan J, Lee KF, Vale W. Urocortin 3 regulates glucose-stimulated insulin secretion and energy homeostasis. Proc Natl Acad Sci U S A. 2007 Mar 6;104(10):4206–11. doi:10.1073/pnas.0611641104 PubMed PMID: 17360501.
18. Lutz TA. The interaction of amylin with other hormones in the control of eating. Diabetes Obes Metab. 2013 Feb 29;15(2):99–111. doi:10.1111/j.1463-1326.2012.01670.x
19. Young AA. Brainstem sensing of meal-related signals in energy homeostasis. Neuropharmacology. 2012 Jul;63(1):31–45. doi:10.1016/j.neuropharm.2012.03.019
20. Ishibashi C, Yoneda S, Fujita Y, Fujita S, Mitsushio K, Ozawa H, et al. Decreased islet amyloid polypeptide staining in the islets of insulinoma patients. Islets. 2024 Dec 31;16(1). doi:10.1080/19382014.2024.2379650
21. Kahn SE, Andrikopoulos S, Verchere CB. Islet amyloid: a long-recognized but underappreciated pathological feature of type 2 diabetes. Diabetes. 1999 Feb 1;48(2):241–53. doi:10.2337/diabetes.48.2.241
22. Zhang XX, Pan YH, Huang YM, Zhao HL. Neuroendocrine hormone amylin in diabetes. World J Diabetes. 2016;7(9):189. doi:10.4239/wjd.v7.i9.189
23. Xu E, Kumar M, Zhang Y, Ju W, Obata T, Zhang N, et al. Intra-islet insulin suppresses glucagon release via GABA-GABAA receptor system. Cell Metab. 2006 Jan;3(1):47–58. doi:10.1016/j.cmet.2005.11.015
24. Gammelsaeter R, Coppola T, Marcaggi P, Storm-Mathisen J, Chaudhry FA, Attwell D, et al. A Role for Glutamate Transporters in the Regulation of Insulin Secretion. PLoS One. 2011 Aug 11;6(8):e22960. doi:10.1371/journal.pone.0022960
25. Almaça J, Molina J, Menegaz D, Pronin AN, Tamayo A, Slepak V, et al. Human Beta Cells Produce and Release Serotonin to Inhibit Glucagon Secretion from Alpha Cells. Cell Rep. 2016 Dec;17(12):3281–91. doi:10.1016/j.celrep.2016.11.072
26. Cai Q, Brissova M, Reinert RB, Cheng Pan F, Brahmachary P, Jeansson M, et al. Enhanced expression of VEGF-A in β cells increases endothelial cell number but impairs islet morphogenesis and β cell proliferation. Dev Biol. 2012 Jul;367(1):40–54. doi:10.1016/j.ydbio.2012.04.022
27. George M, Ayuso E, Casellas A, Costa C, Devedjian JC, Bosch F. β cell expression of IGF-I leads to recovery from type 1 diabetes. Journal of Clinical Investigation. 2002 May 1;109(9):1153–63. doi:10.1172/JCI12969
28. Sétula C, Pensado-Evans I, Scelza-Figueredo A, Orellano MS, Rodríguez-Valero I, Spinedi E, et al. IL-1β priming triggers an adaptive stress response that enhances pancreatic β-cell resilience to subsequent cytotoxic inflammatory insult. Cell Death Dis. 2025 Oct 21;16(1):744. doi:10.1038/s41419-025-08059-0
29. Marasco MR, Conteh AM, Reissaus CA, Cupit JE, Appleman EM, Mirmira RG, et al. Interleukin-6 Reduces β-Cell Oxidative Stress by Linking Autophagy With the Antioxidant Response. Diabetes. 2018 Aug 1;67(8):1576–88. doi:10.2337/db17-1280
30. Flisher MF, Shin D, Huising MO. Urocortin3: Local inducer of somatostatin release and bellwether of beta cell maturity. Peptides (NY). 2022 May;151:170748. doi:10.1016/j.peptides.2022.170748
31. Bartolomé A. The Pancreatic Beta Cell: Editorial. Biomolecules. 2023 Mar 8;13(3). doi:10.3390/biom13030495 PubMed PMID: 36979430.

32. Fridlyand LE, Philipson LH. Glucose sensing in the pancreatic beta cell: a computational systems analysis. Theor Biol Med Model. 2010 May 24;7:15. doi:10.1186/1742-4682-7-15 PubMed PMID: 20497556.
33. Ashcroft FM, Lloyd M, Haythorne EA. Glucokinase activity in diabetes: too much of a good thing? Trends in Endocrinology & Metabolism. 2023 Feb;34(2):119–30. doi:10.1016/j.tem.2022.12.007
34. Rorsman P, Ashcroft FM. Pancreatic β-Cell Electrical Activity and Insulin Secretion: Of Mice and Men. Physiol Rev. 2018 Jan 1;98(1):117–214. doi:10.1152/physrev.00008.2017
35. Swarup S, Ahmed I, Grigorova Y, Zeltser R. Metabolic Syndrome. 2026. PubMed PMID: 29083742.
36. Butler AE, Janson J, Bonner-Weir S, Ritzel R, Rizza RA, Butler PC. β-Cell Deficit and Increased β-Cell Apoptosis in Humans With Type 2 Diabetes. Diabetes. 2003 Jan 1;52(1):102–10. doi:10.2337/diabetes.52.1.102
37. Kahn SE, Hull RL, Utzschneider KM. Mechanisms linking obesity to insulin resistance and type 2 diabetes. Nature. 2006 Dec 13;444(7121):840–6. doi:10.1038/nature05482
38. Itani SI, Ruderman NB, Schmieder F, Boden G. Lipid-Induced Insulin Resistance in Human Muscle Is Associated With Changes in Diacylglycerol, Protein Kinase C, and IκB-α. Diabetes. 2002 Jul 1;51(7):2005–11. doi:10.2337/diabetes.51.7.2005
39. Samuel VT, Liu ZX, Qu X, Elder BD, Bilz S, Befroy D, et al. Mechanism of Hepatic Insulin Resistance in Non-alcoholic Fatty Liver Disease. Journal of Biological Chemistry. 2004 Jul;279(31):32345–53. doi:10.1074/jbc.M313478200
40. Holland WL, Brozinick JT, Wang LP, Hawkins ED, Sargent KM, Liu Y, et al. Inhibition of Ceramide Synthesis Ameliorates Glucocorticoid-, Saturated-Fat-, and Obesity-Induced Insulin Resistance. Cell Metab. 2007 Mar;5(3):167–79. doi:10.1016/j.cmet.2007.01.002
41. Samuel VT, Shulman GI. Mechanisms for Insulin Resistance: Common Threads and Missing Links. Cell. 2012 Mar;148(5):852–71. doi:10.1016/j.cell.2012.02.017
42. Brownlee M. The Pathobiology of Diabetic Complications. Diabetes. 2005 Jun 1;54(6):1615–25. doi:10.2337/diabetes.54.6.1615
43. Robertson RP, Harmon JS. Diabetes, glucose toxicity, and oxidative stress: A case of double jeopardy for the pancreatic islet β cell. Free Radic Biol Med. 2006 Jul;41(2):177–84. doi:10.1016/j.freeradbiomed.2005.04.030
44. Ramasamy R, Yan SF, Schmidt AM. Receptor for AGE (RAGE): signaling mechanisms in the pathogenesis of diabetes and its complications. Ann N Y Acad Sci. 2011 Dec 23;1243(1):88–102. doi:10.1111/j.1749-6632.2011.06320.x
45. Nishikawa T, Edelstein D, Du XL, Yamagishi S ichi, Matsumura T, Kaneda Y, et al. Normalizing mitochondrial superoxide production blocks three pathways of hyperglycaemic damage. Nature. 2000 Apr;404(6779):787–90. doi:10.1038/35008121
46. Hudish LI, Reusch JE, Sussel L. β Cell dysfunction during progression of metabolic syndrome to type 2 diabetes. J Clin Invest. 2019 Oct 1;129(10):4001–8. doi:10.1172/JCI129188 PubMed PMID: 31424428.
47. Supale S, Li N, Brun T, Maechler P. Mitochondrial dysfunction in pancreatic β cells. Trends in Endocrinology & Metabolism. 2012 Sep;23(9):477–87. doi:10.1016/j.tem.2012.06.002
48. Gerber PA, Rutter GA. The Role of Oxidative Stress and Hypoxia in Pancreatic Beta-Cell Dysfunction in Diabetes Mellitus. Antioxid Redox Signal. 2017 Apr 1;26(10):501–18. doi:10.1089/ars.2016.6755

49. Jonas JC, Sharma A, Hasenkamp W, Ilkova H, Patanè G, Laybutt R, et al. Chronic Hyperglycemia Triggers Loss of Pancreatic β Cell Differentiation in an Animal Model of Diabetes. Journal of Biological Chemistry. 1999 May;274(20):14112–21. doi:10.1074/jbc.274.20.14112
50. Weir GC, Bonner-Weir S. Five Stages of Evolving Beta-Cell Dysfunction During Progression to Diabetes. Diabetes. 2004 Dec 1;53(suppl_3):S16–21. doi:10.2337/diabetes.53.suppl_3.S16
51. Arner E, Westermark PO, Spalding KL, Britton T, Rydén M, Frisén J, et al. Adipocyte Turnover: Relevance to Human Adipose Tissue Morphology. Diabetes. 2010 Jan 1;59(1):105–9. doi:10.2337/db09-0942
52. Lee YS, Kim JW, Osborne O, Oh DY, Sasik R, Schenk S, et al. Increased adipocyte O2 consumption triggers HIF-1α, causing inflammation and insulin resistance in obesity. Cell. 2014 Jun 5;157(6):1339–52. doi:10.1016/j.cell.2014.05.012 PubMed PMID: 24906151.
53. Stienstra R, Joosten LAB, Koenen T, van Tits B, van Diepen JA, van den Berg SAA, et al. The Inflammasome-Mediated Caspase-1 Activation Controls Adipocyte Differentiation and Insulin Sensitivity. Cell Metab. 2010 Dec;12(6):593–605. doi:10.1016/j.cmet.2010.11.011
54. Hotamisligil GS. Inflammation and metabolic disorders. Nature. 2006 Dec 14;444(7121):860–7. doi:10.1038/nature05485
55. Wilmanski JM, Petnicki-Ocwieja T, Kobayashi KS. NLR proteins: integral members of innate immunity and mediators of inflammatory diseases. J Leukoc Biol. 2008 Jan 1;83(1):13–30. doi:10.1189/jlb.0607402
56. Pétrilli V, Dostert C, Muruve DA, Tschopp J. The inflammasome: a danger sensing complex triggering innate immunity. Curr Opin Immunol. 2007 Dec;19(6):615–22. doi:10.1016/j.coi.2007.09.002
57. Chen MC, Meckfessel MH. Autoinflammatory Disorders, Pain, and Neural Regulation of Inflammation. Dermatol Clin. 2013 Jul;31(3):461–70. doi:10.1016/j.det.2013.04.002
58. Sollberger G, Strittmatter GE, Garstkiewicz M, Sand J, Beer HD. Caspase-1: The inflammasome and beyond. Innate Immun. 2014 Feb 15;20(2):115–25. doi:10.1177/1753425913484374
59. Ramachandran R, Manan A, Kim J, Choi S. NLRP3 inflammasome: a key player in the pathogenesis of life-style disorders. Exp Mol Med. 2024 Jul 1;56(7):1488–500. doi:10.1038/s12276-024-01261-8
60. Mo Y, Mo L, Zhang Y, Zhang Y, Yuan J, Zhang Q. High glucose enhances the activation of NLRP3 inflammasome by ambient fine particulate matter in alveolar macrophages. Part Fibre Toxicol. 2023 Nov 2;20(1):41. doi:10.1186/s12989-023-00552-8 PubMed PMID: 37919797.
61. Wen H, Gris D, Lei Y, Jha S, Zhang L, Huang MTH, et al. Fatty acid–induced NLRP3-ASC inflammasome activation interferes with insulin signaling. Nat Immunol. 2011 May 10;12(5):408–15. doi:10.1038/ni.2022
62. Moretti J, Jia B, Hutchins Z, Roy S, Yip H, Wu J, et al. Caspase-11 interaction with NLRP3 potentiates the noncanonical activation of the NLRP3 inflammasome. Nat Immunol. 2022 May 29;23(5):705–17. doi:10.1038/s41590-022-01192-4
63. Lacey CA, Mitchell WJ, Dadelahi AS, Skyberg JA. Caspase-1 and Caspase-11 Mediate Pyroptosis, Inflammation, and Control of Brucella Joint Infection. Infect Immun. 2018 Sep;86(9). doi:10.1128/IAI.00361-18

64. Ng TM, Monack DM. Revisiting Caspase-11 Function in Host Defense. Cell Host Microbe. 2013 Jul;14(1):9–14. doi:10.1016/j.chom.2013.06.009
65. Denes A, Lopez-Castejon G, Brough D. Caspase-1: is IL-1 just the tip of the ICEberg? Cell Death Dis. 2012 Jul 5;3(7):e338–e338. doi:10.1038/cddis.2012.86
66. Morrison MC, Mulder P, Salic K, Verheij J, Liang W, van Duyvenvoorde W, et al. Intervention with a caspase-1 inhibitor reduces obesity-associated hyperinsulinemia, non-alcoholic steatohepatitis and hepatic fibrosis in LDLR−/−.Leiden mice. Int J Obes. 2016 Sep 28;40(9):1416–23. doi:10.1038/ijo.2016.74
67. Wang H, Capell W, Yoon JH, Faubel S, Eckel RH. Obesity development in caspase-1-deficient mice. Int J Obes. 2014 Jan 24;38(1):152–5. doi:10.1038/ijo.2013.59
68. Kimura H, Karasawa T, Usui F, Kawashima A, Endo Y, Kobayashi M, et al. Caspase-1 deficiency promotes high-fat diet-induced adipose tissue inflammation and the development of obesity. American Journal of Physiology-Endocrinology and Metabolism. 2016 Nov 1;311(5):E881–90. doi:10.1152/ajpendo.00174.2016
69. Dixon LJ, Flask CA, Papouchado BG, Feldstein AE, Nagy LE. Caspase-1 as a Central Regulator of High Fat Diet-Induced Non-Alcoholic Steatohepatitis. PLoS One. 2013 Feb 7;8(2):e56100. doi:10.1371/journal.pone.0056100
70. Dominy J, Koch C, Arnold C, George V, Khan MZ, Khalid S, et al. Caspase 1–deficient humans survive into late adulthood despite dramatically lower canonical inflammasome activity. Journal of Allergy and Clinical Immunology. 2026 Jan;157(1):217–25. doi:10.1016/j.jaci.2025.09.025
71. Palomäki VA, Väyrynen JP, Koivukangas V, Meriläinen S, Karttunen TJ, Lehenkari P. NLRP3-Caspase-1 Axis in Human Adipose Tissue Crown-Like Structures: A Potential Mediator of Inflammation and the Effects of Bariatric Surgery. Immun Inflamm Dis. 2026 Feb 5;14(2). doi:10.1002/iid3.70312
72. Everett BM, Donath MY, Pradhan AD, Thuren T, Pais P, Nicolau JC, et al. Anti-Inflammatory Therapy With Canakinumab for the Prevention and Management of Diabetes. J Am Coll Cardiol. 2018 May;71(21):2392–401. doi:10.1016/j.jacc.2018.03.002
73. Thornberry NA, Lazebnik Y. Caspases: Enemies Within. Science (1979). 1998 Aug 28;281(5381):1312–6. doi:10.1126/science.281.5381.1312
74. Ashkenazi A, Salvesen G. Regulated Cell Death: Signaling and Mechanisms. Annu Rev Cell Dev Biol. 2014 Oct 11;30(1):337–56. doi:10.1146/annurev-cellbio-100913-013226
75. Salvesen GS, Ashkenazi A. SnapShot: Caspases. Cell. 2011 Nov;147(5):1197. doi:10.1016/j.cell.2011.11.007
76. Galluzzi L, Vitale I, Aaronson SA, Abrams JM, Adam D, Agostinis P, et al. Molecular mechanisms of cell death: recommendations of the Nomenclature Committee on Cell Death 2018. Cell Death Differ. 2018 Mar 23;25(3):486–541. doi:10.1038/s41418-017-0012-4
77. Vanlangenakker N, Vanden Berghe T, Vandenabeele P. Many stimuli pull the necrotic trigger, an overview. Cell Death Differ. 2012 Jan 11;19(1):75–86. doi:10.1038/cdd.2011.164
78. Vercammen D, Beyaert R, Denecker G, Goossens V, Van Loo G, Declercq W, et al. Inhibition of Caspases Increases the Sensitivity of L929 Cells to Necrosis Mediated by Tumor Necrosis Factor. J Exp Med. 1998 May 4;187(9):1477–85. doi:10.1084/jem.187.9.1477

79. Ye K, Chen Z, Xu Y. The double-edged functions of necroptosis. Cell Death Dis. 2023 Feb 27;14(2):163. doi:10.1038/s41419-023-05691-6
80. Newton K. RIPK1 and RIPK3: critical regulators of inflammation and cell death. Trends Cell Biol. 2015 Jun;25(6):347–53. doi:10.1016/j.tcb.2015.01.001
81. Bergsbaken T, Fink SL, Cookson BT. Pyroptosis: host cell death and inflammation. Nat Rev Microbiol. 2009 Feb;7(2):99–109. doi:10.1038/nrmicro2070
82. Xu Y, Ma H, Shao J, Wu J, Zhou L, Zhang Z, et al. A Role for Tubular Necroptosis in Cisplatin-Induced AKI. Journal of the American Society of Nephrology. 2015 Nov;26(11):2647–58. doi:10.1681/ASN.2014080741
83. Lin J, Li H, Yang M, Ren J, Huang Z, Han F, et al. A Role of RIP3-Mediated Macrophage Necrosis in Atherosclerosis Development. Cell Rep. 2013 Jan;3(1):200–10. doi:10.1016/j.celrep.2012.12.012
84. Yuan J, Amin P, Ofengeim D. Necroptosis and RIPK1-mediated neuroinflammation in CNS diseases. Nat Rev Neurosci. 2019 Jan 22;20(1):19–33. doi:10.1038/s41583-018-0093-1
85. Cao T, Ni R, Ding W, Ji X, Li L, Liao G, et al. MLKL-mediated necroptosis is a target for cardiac protection in mouse models of type-1 diabetes. Cardiovasc Diabetol. 2022 Aug 27;21(1):165. doi:10.1186/s12933-022-01602-9
86. Yang B, Maddison LA, Zaborska KE, Dai C, Yin L, Tang Z, et al. RIPK3-mediated inflammation is a conserved β cell response to ER stress. Sci Adv. 2020 Dec 18;6(51). doi:10.1126/sciadv.abd7272
87. Shutinoski B, Patel R, Tomlinson JJ, Schlossmacher MG, Sad S. Ripk3 licenced protection against microbial infection in the absence of Caspase1-11 inflammasome. Microbes Infect. 2020 Jan;22(1):40–5. doi:10.1016/j.micinf.2019.08.002
88. Denroche HC, Miard S, Sallé-Lefort S, Picard F, Verchere CB. T cells accumulate in non-diabetic islets during ageing. Immunity & Ageing. 2021 Dec 23;18(1):8. doi:10.1186/s12979-021-00221-4
89. Kuida K, Lippke JA, Ku G, Harding MW, Livingston DJ, Su MSS, et al. Altered Cytokine Export and Apoptosis in Mice Deficient in Interleukin-1β Converting Enzyme. Science (1979). 1995 Mar 31;267(5206):2000–3. doi:10.1126/science.7535475
90. Newton K, Sun X, Dixit VM. Kinase RIP3 Is Dispensable for Normal NF-κBs, Signaling by the B-Cell and T-Cell Receptors, Tumor Necrosis Factor Receptor 1, and Toll-Like Receptors 2 and 4. Mol Cell Biol. 2004 Feb 1;24(4):1464–9. doi:10.1128/MCB.24.4.1464-1469.2004
91. Rauch I, Deets KA, Ji DX, von Moltke J, Tenthorey JL, Lee AY, et al. NAIP-NLRC4 Inflammasomes Coordinate Intestinal Epithelial Cell Expulsion with Eicosanoid and IL-18 Release via Activation of Caspase-1 and -8. Immunity. 2017 Apr;46(4):649–59. doi:10.1016/j.immuni.2017.03.016
92. Mina AI, LeClair RA, LeClair KB, Cohen DE, Lantier L, Banks AS. CalR: A Web-Based Analysis Tool for Indirect Calorimetry Experiments. Cell Metab. 2018 Oct;28(4):656-666.e1. doi:10.1016/j.cmet.2018.06.019
93. Ibrahim M, MacFarlane EM, Matteo G, Hoyeck MP, Rick KRC, Farokhi S, et al. Functional cytochrome P450 1A enzymes are induced in mouse and human islets following pollutant exposure. Diabetologia. 2020 Jan 27;63(1):162–78. doi:10.1007/s00125-019-05035-0

94. Livak KJ, Schmittgen TD. Analysis of Relative Gene Expression Data Using Real-Time Quantitative PCR and the 2−ΔΔCT Method. Methods. 2001 Dec;25(4):402–8. doi:10.1006/meth.2001.1262
95. van Allen KA, Gang N, Hoyeck MP, Perera I, Zhang D, Atlas E, et al. Characterizing the effects of Dechlorane Plus on β-cells: a comparative study across models and species. Islets. 2024 Dec 31;16(1). doi:10.1080/19382014.2024.2361996
96. Shiao MS, Liao BY, Long M, Yu HT. Adaptive Evolution of the Insulin Two-Gene System in Mouse. Genetics. 2008 Mar 1;178(3):1683–91. doi:10.1534/genetics.108.087023
97. Nishimura W, Iwasa H, Tumurkhuu M. Role of the Transcription Factor MAFA in the Maintenance of Pancreatic β-Cells. Int J Mol Sci. 2022 Apr 19;23(9):4478. doi:10.3390/ijms23094478
98. Taylor BL, Liu FF, Sander M. Nkx6.1 Is Essential for Maintaining the Functional State of Pancreatic Beta Cells. Cell Rep. 2013 Sep;4(6):1262–75. doi:10.1016/j.celrep.2013.08.010
99. Matschinsky FM, Wilson DF. The Central Role of Glucokinase in Glucose Homeostasis: A Perspective 50 Years After Demonstrating the Presence of the Enzyme in Islets of Langerhans. Front Physiol. 2019 Mar 6;10. doi:10.3389/fphys.2019.00148
100. Thorens B, Charron MJ, Lodish HF. Molecular Physiology of Glucose Transporters. Diabetes Care. 1990 Mar 1;13(3):209–18. doi:10.2337/diacare.13.3.209
101. Wong W. Pancreatic crosstalk among beta and delta cells. Sci Signal. 2015 Jul 28;8(387). doi:10.1126/scisignal.aad0908
102. Hang Y, Stein R. MafA and MafB activity in pancreatic β cells. Trends in Endocrinology & Metabolism. 2011 Sep;22(9):364–73. doi:10.1016/j.tem.2011.05.003
103. Huang X, Feng Y, Xiong G, Whyte S, Duan J, Yang Y, et al. Caspase-11, a specific sensor for intracellular lipopolysaccharide recognition, mediates the non-canonical inflammatory pathway of pyroptosis. Cell Biosci. 2019 Dec 27;9(1):31. doi:10.1186/s13578-019-0292-0
104. Bouzakri K, Plomgaard P, Berney T, Donath MY, Pedersen BK, Halban PA. Bimodal Effect on Pancreatic β-Cells of Secretory Products From Normal or Insulin-Resistant Human Skeletal Muscle. Diabetes. 2011 Apr 1;60(4):1111–21. doi:10.2337/db10-1178
105. Langlois A, Dumond A, Vion J, Pinget M, Bouzakri K. Crosstalk Communications Between Islets Cells and Insulin Target Tissue: The Hidden Face of Iceberg. Front Endocrinol (Lausanne). 2022;13:836344. doi:10.3389/fendo.2022.836344 PubMed PMID: 35185804.
106. Cabrera O, Ficorilli J, Shaw J, Echeverri F, Schwede F, Chepurny OG, et al. Intra-islet glucagon confers β-cell glucose competence for first-phase insulin secretion and favors GLP-1R stimulation by exogenous glucagon. Journal of Biological Chemistry. 2022 Feb;298(2):101484. doi:10.1016/j.jbc.2021.101484
107. Zhu L, Dattaroy D, Pham J, Wang L, Barella LF, Cui Y, et al. Intraislet glucagon signaling is critical for maintaining glucose homeostasis. JCI Insight. 2019 May 16;4(10). doi:10.1172/jci.insight.127994
108. Gonzalez A, Merino B, Marroquí L, Ñeco P, Alonso-Magdalena P, Caballero-Garrido E, et al. Insulin Hypersecretion in Islets From Diet-Induced Hyperinsulinemic Obese Female Mice Is Associated With Several Functional Adaptations in Individual β-Cells. Endocrinology. 2013 Oct 1;154(10):3515–24. doi:10.1210/en.2013-1424

109. Zhang T, Kim DH, Xiao X, Lee S, Gong Z, Muzumdar R, et al. FoxO1 Plays an Important Role in Regulating β-Cell Compensation for Insulin Resistance in Male Mice. Endocrinology. 2016 Mar 1;157(3):1055–70. doi:10.1210/en.2015-1852
110. Zhang C, Moriguchi T, Kajihara M, Esaki R, Harada A, Shimohata H, et al. MafA Is a Key Regulator of Glucose-Stimulated Insulin Secretion. Mol Cell Biol. 2005 Jun 27;25(12):4969–76. doi:10.1128/MCB.25.12.4969-4976.2005
111. Nadendla EK, Tweedell RE, Kasof G, Kanneganti TD. Caspases: structural and molecular mechanisms and functions in cell death, innate immunity, and disease. Cell Discov. 2025 May 5;11(1):42. doi:10.1038/s41421-025-00791-3
112. Shi J, Zhao Y, Wang Y, Gao W, Ding J, Li P, et al. Inflammatory caspases are innate immune receptors for intracellular LPS. Nature. 2014 Oct 6;514(7521):187–92. doi:10.1038/nature13683
113. Kayagaki N, Warming S, Lamkanfi M, Walle L Vande, Louie S, Dong J, et al. Non-canonical inflammasome activation targets caspase-11. Nature. 2011 Nov 16;479(7371):117–21. doi:10.1038/nature10558
114. Wang S, Miura M, Jung Y keun, Zhu H, Li E, Yuan J. Murine Caspase-11, an ICE-Interacting Protease, Is Essential for the Activation of ICE. Cell. 1998 Feb;92(4):501–9. doi:10.1016/S0092-8674(00)80943-5
115. Saeed WK, Jun DW, Jang K, Ahn SB, Oh JH, Chae YJ, et al. Mismatched effects of receptor interacting protein kinase-3 on hepatic steatosis and inflammation in non-alcoholic fatty liver disease. World J Gastroenterol. 2018 Dec 28;24(48):5477–90. doi:10.3748/wjg.v24.i48.5477
116. Xu H, Du X, Liu G, Huang S, Du W, Zou S, et al. The pseudokinase MLKL regulates hepatic insulin sensitivity independently of inflammation. Mol Metab. 2019 May;23:14–23. doi:10.1016/j.molmet.2019.02.003
117. Jo S, Beetch M, Gustafson E, Wong A, Oribamise E, Chung G, et al. Sex Differences in Pancreatic β-Cell Physiology and Glucose Homeostasis in C57BL/6J Mice. J Endocr Soc. 2023 Aug 2;7(9). doi:10.1210/jendso/bvad099
118. Benedé-Ubieto R, Estévez-Vázquez O, Ramadori P, Cubero FJ, Nevzorova YA. Guidelines and Considerations for Metabolic Tolerance Tests in Mice . Diabetes Metab Syndr Obes. 2020 Feb;Volume 13:439–50. doi:10.2147/DMSO.S234665
119. Justice MJ. Sex matters in preclinical research. Dis Model Mech. 2024 Mar 1;17(3). doi:10.1242/dmm.050759
120. Moro C, Magnan C. Revisited guidelines for metabolic tolerance tests in mice. Lab Anim (NY). 2025 Jan 25;54(1):16–23. doi:10.1038/s41684-024-01473-5
121. Stamateris RE, Sharma RB, Hollern DA, Alonso LC. Adaptive β-cell proliferation increases early in high-fat feeding in mice, concurrent with metabolic changes, with induction of islet cyclin D2 expression. American Journal of Physiology-Endocrinology and Metabolism. 2013 Jul 1;305(1):E149–59. doi:10.1152/ajpendo.00040.2013
122. Ahrén J, Ahrén B, Wierup N. Increased β-cell volume in mice fed a high-fat diet: A dynamic study over 12 months. Islets. 2010 Nov 27;2(6):353–6. doi:10.4161/isl.2.6.13619
123. Collins SC, Hoppa MB, Walker JN, Amisten S, Abdulkader F, Bengtsson M, et al. Progression of Diet-Induced Diabetes in C57BL6J Mice Involves Functional Dissociation of Ca2+ Channels From Secretory Vesicles. Diabetes. 2010 May 1;59(5):1192–201. doi:10.2337/db09-0791

124. Schreiber V. [Endocrinology 1992-1993]. Cas Lek Cesk. 1994 Apr 18;133(8):235–6. PubMed PMID: 8194086.
125. Eychenne R, Bouvry C, Bourgeois M, Loyer P, Benoist E, Lepareur N. Overview of Radiolabeled Somatostatin Analogs for Cancer Imaging and Therapy. Molecules. 2020 Sep 2;25(17):4012. doi:10.3390/molecules25174012
126. Noguchi GM, Castillo VC, Donaldson CJ, Flisher MR, Momen AT, Saghatelian A, et al. Urocortin 3 contributes to paracrine inhibition of islet alpha cells in mice. Journal of Endocrinology. 2024 Apr 8;261(3). doi:10.1530/JOE-24-0018

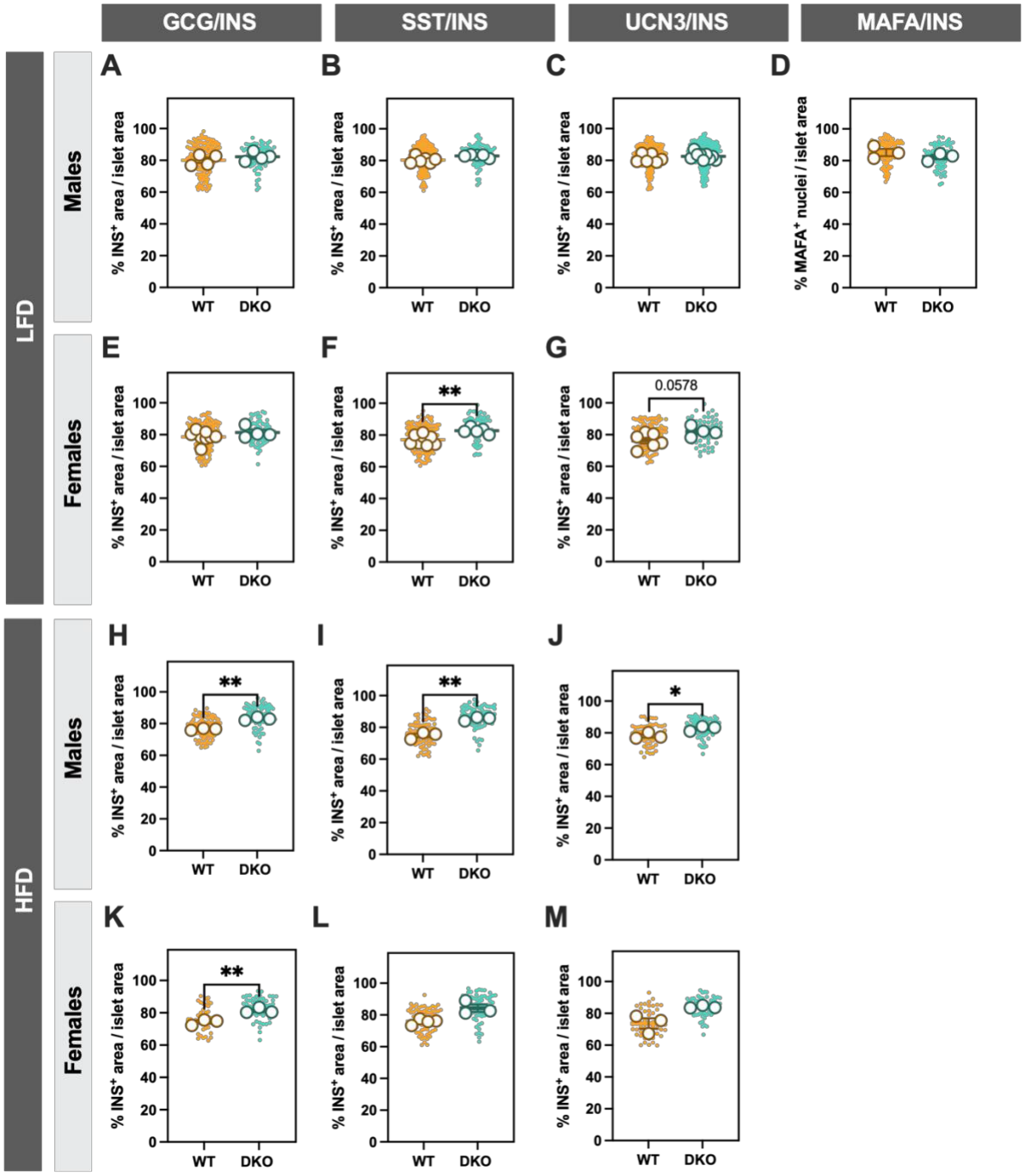

Supplemental Figure 1. IF replicates of insulin quantification per stain.
(A-M) IF insulin-stained replicates of paraffin-embedded pancreatic sections were co-stained with either glucagon (GCG)/insulin, somatostatin (SST)/insulin, UCN3/insulin, or MAFA/insulin. Small, light-colored dots represent quantified individual islets (5-59 per mouse), while large, dark-colored dots indicate the average of all islets per mouse (n = 3-9 mice per genotype). Data are presented as mean ± SEM. Statistical significance was determined using an unpaired, two-tailed Welch's t-test. *$p < 0.05$, ****$p < 0.0001$.

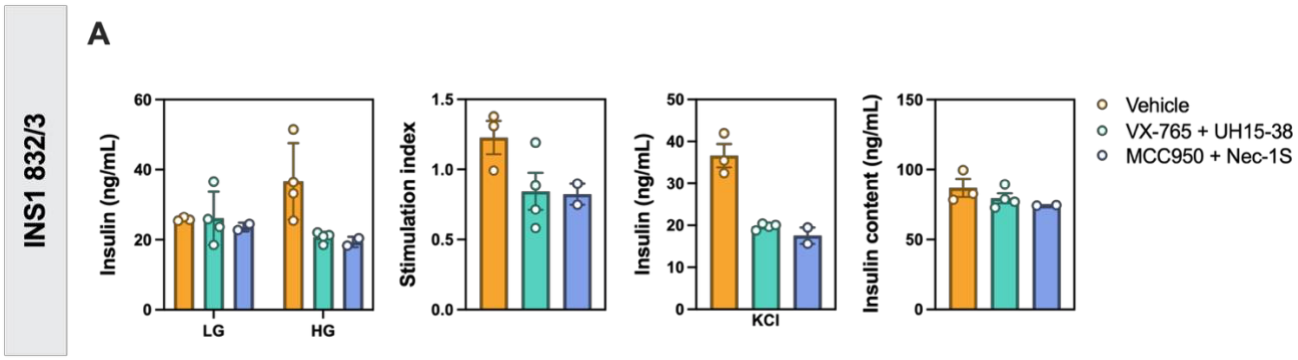

Supplemental Figure 2. Pharmacological inhibition of Casp1/Ripk3 in INS1 832/3 cells.
(A) Static GSIS was performed following a 24-hour treatment with inhibitors of Casp1 (VX-765, 2.5 μM), Ripk3 (UH15-38, 2.5 μM), the NLRP3 inflammasome (MCC-950, 2.5 μM), or Ripk1 (Nec1s, 2.5 μM). GSIS was assessed following 1-hour incubations in low glucose (LG; 2.8 mM), high glucose (HG; 16.7 mM), and depolarizing potassium chloride (KCl; 30 mM). The stimulation index was calculated as the ratio of insulin secretion under HG relative to LG conditions. Total insulin content was collected following overnight incubation in acid ethanol. Data are presented as mean ± SEM (n = 2-4 replicates per group).

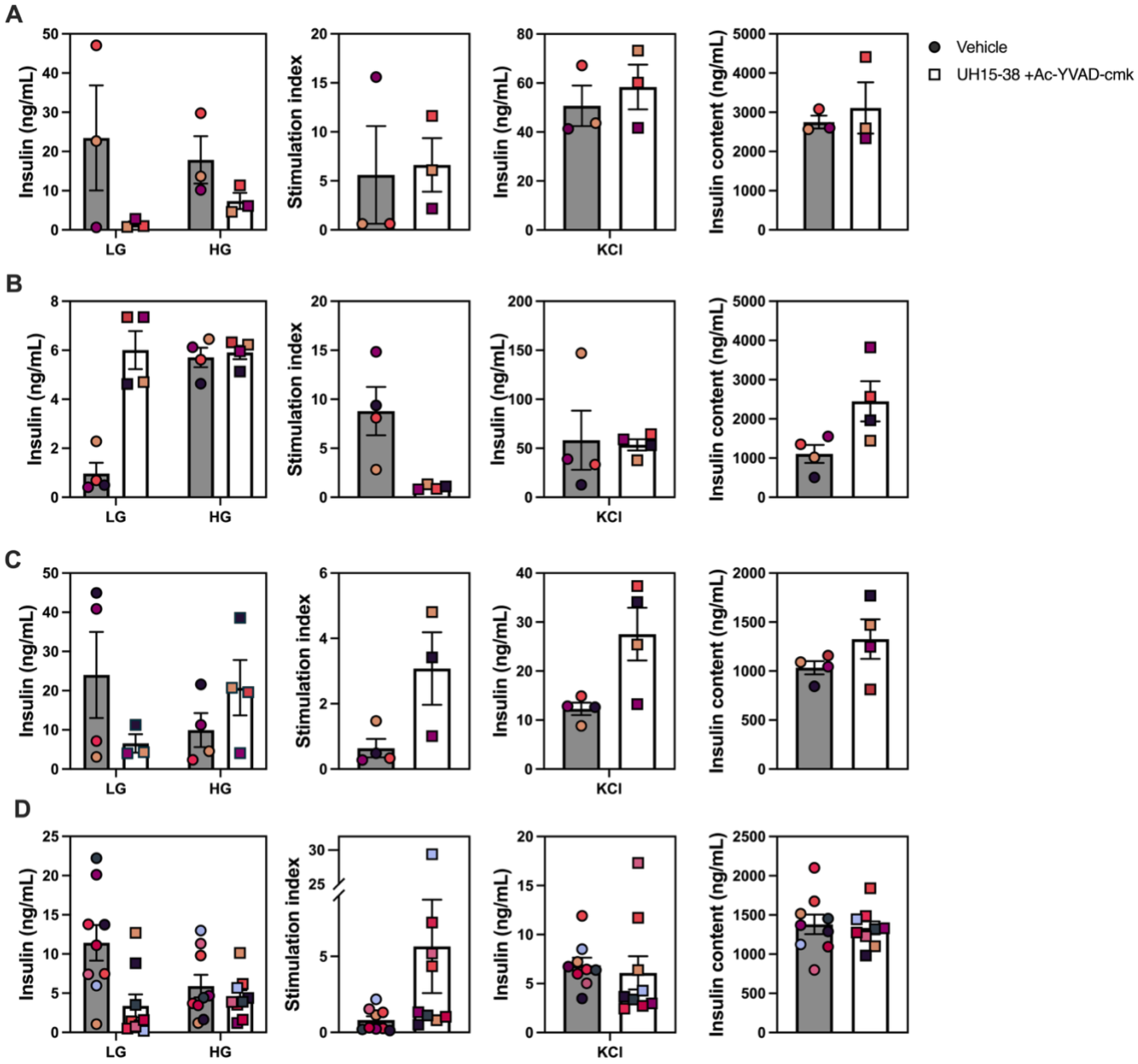

Supplemental Figure 3. Pharmacological inhibition of Casp1/Ripk3 in isolated islets during static GSIS.

(A-D) Replicates of static insulin secretion from isolated islets of C57BL/6J male and female mice following a 24-hour treatment with either vehicle (0.02 % DMSO) or Casp1 (VX-765, 0.5 μM) and Ripk3 (UH15-38, 0.5 μM) inhibitors. GSIS was measured following 1-hour incubations in low glucose (LG; 2.8 mM), high glucose (HG; 16.7 mM), and depolarizing potassium (KCl; 30 mM). The stimulation index was calculated as the ratio of insulin secretion at HG to LG. Total insulin content was collected from overnight incubation in acid ethanol. Data are mean ± SEM (n = 3-9 mice per genotype).